Measurement report: Regional characteristics of seasonal and long-term variations in greenhouse gases at Nainital, India and Comilla, Bangladesh

Shohei Nomura[1], Manish Naja[2], Md. Kawser Ahmed[3], Hitoshi Mukai[1], Yukio Terao[1], Toshinobu Machida[1], Motoki Sasakawa[1], Prabir K. Patra[4]

[1]Center for Global Environmental Research, National Institute for Environmental Studies, 16-2 Onogawa, Tsukuba, Ibaraki, 305-8506, Japan
[2]Aryabhatta Research Institute of Observational Sciences, Manora Peak, Nainital Uttarakhand 263129, India
[3]Department of Oceanography, Faculty of Earth & Environmental Sciences, University of Dhaka, Dhaka-1000, Bangladesh
[4]Research Institute for Global Change, JAMSTEC, 3173-25 Showa-machi, Yokohama, 236-0001, Japan

Correspondence to: Shohei Nomura (nomura.shohei@nies.go.jp) Tel.: +81 298502370; fax: +81 298502960

Abstract

Emissions of greenhouse gases (GHGs) from the Indian subcontinent have increased during the last 20 years along with rapid economic growth, however, there remains a paucity of GHG measurements for policy relevant research. In northern India and Bangladesh, agricultural activities are considered to play an important role on GHGs concentrations in the atmosphere. We performed weekly air sampling at Nainital (NTL) in northern India and Comilla (CLA) in Bangladesh from 2006 and 2012, respectively. Air samples were analyzed for dry-air gas mole fractions of CO_2, CH_4, CO, H_2, N_2O, and SF_6, and carbon and oxygen isotopic ratios of CO_2 ($\delta^{13}C$-CO_2 and $\delta^{18}O$-CO_2). Regional characteristics of these components over the Indo-Gangetic Plain are discussed compared to data from other Indian sites and Mauna Loa, Hawaii (MLO), which is representative of marine background air.

We found that the CO_2 mole fraction at CLA had two seasonal minima in February–March and September, corresponding to crop cultivation activities that depend on regional climatic conditions. Although NTL had only one clear minima in September, the carbon isotopic signature suggested that photosynthetic CO_2 absorption by crops cultivated in each season contributes differently to lower CO_2 mole fractions at both sites. The CH_4 mole fraction of NTL and CLA in August–October showed high values (i.e., sometimes over 4,000 ppb at CLA) mainly due to the influence of CH_4 emissions from the paddy fields. High CH_4 mole fractions sustained over months at CLA were a characteristic feature in the Indo-Gangetic Plain, which were affected by the both local emission and air mass transport. The CO mole fractions at NTL were also high and showed peaks in May and October, while CLA had much higher peaks in October–March due to the influence of human activities such as emissions from biomass burning and brick production. The N_2O mole fractions at NTL and CLA increased in June–August and November–February, which coincided with the application of nitrogen fertilizer and the burning of biomass such as the harvest residues and dung for domestic cooking. Based on H_2 seasonal variation at both sites, it appeared that the emissions in this region were related to biomass burning in addition to production from the reaction of OH and CH_4. The SF_6 mole fraction was similar to that at MLO, suggesting that there were few anthropogenic SF_6 emission sources in the district.

The variability of CO_2 growth rate at NTL was different from the variability in the CO_2 growth rate at MLO, which is more closely linked with the El Niño Southern Oscillation (ENSO). In addition, the growth rates of the CH_4 and SF_6 mole fractions at NTL showed an anticorrelation with those at MLO, indicating that the frequency of southerly air masses strongly influenced these mole fractions. These finding showed that rather large regional climatic conditions considerably controlled interannual variations in GHGs, $\delta^{13}C$-CO_2, and $\delta^{18}O$-CO_2 through changes in precipitation and air mass.

Keywords

Northern India, Bangladesh, Greenhouse gases variation, Isotope ratio of CO_2, Local emissions

1 Introduction

The mole fraction of many greenhouse gases (GHGs) in the atmosphere, including CO_2, CH_4, and N_2O, has been increasing worldwide in recent years. As for CO_2, rapid increases in CO_2 emissions from developing countries contribute strongly to acceleration of the growth rate of its mole fraction (Friedlingstein et al., 2019). For instance, anthropogenic CO_2 emission of India has increased in 2017 it reached to 2.45 $GtCO_2$ yr^{-1} which was the third highest in the world (Muntean et al., 2018). Therefore, South Asian region must be important to evaluate GHG in the future. Patra et al. (2013) calculated the CO_2 flux in South Asia using top-down and bottom-up methods and reported that CO_2 fluxes in top-down and bottom-up were –104 ± 150 $TgCyr^{-1}$ and –191 ± 193 $TgCyr^{-1}$. In other words, CO_2 was absorbed in South Asia, however, the error of CO_2 flux was very large because there are only a few measured GHG moles fractions in the South Asian region.

The first systematic monitoring for GHGs mole fractions and carbon isotopic ratio in the South Asian region was performed by Bhattacharya et al. (2009). They carried out monitoring at Cape Rama station (CRI) (15.1°N, 73.9°E, 60 m a.s.l.) on the West Coast of India from 1993 and found that (1) the CH_4 and CO mole fractions increased in October–March when the air mass came from the northeast (inland), and decreased in June–August when the air mass came from southwest (ocean); (2) the CO_2, CH_4, CO, H_2 and N_2O mole fractions in June–August were generally at the same levels at the background sites at the observatory in Seychelles Island and Hawaii Island; (3) the seasonal cycle and phase in CH_4 and CO mole fractions were quite similar and their correlation coefficient was high, generally because they originated from anthropogenic emissions in India. Therefore, it became clear that GHG mole fractions are greatly changed by the seasonal wind and that the Indian subcontinent has strong CH_4 and CO emissions.

In recent decades, a few more research groups have commenced flask sampling or continuous GHG measurements in India. Sharma et al. (2013) measured atmospheric CO_2 mole fractions at Dehradun in northern India in 2009 and detected that the CO_2 mole fraction decreased twice a year (March and September) due to vegetation activity. Ganesan et al. (2013) measured the CH_4, N_2O, and SF_6 mole fractions in December 2011 to February 2013 at Darjeeling in northeastern India and found that (1) CH_4 mole fractions had a positive correlation with the N_2O mole fraction, and that those mole fractions increased due to emissions from anthropogenic activities when air masses came from the Indo-Gangetic Plain; (2) SF_6 emissions in the region showed a weak signal. Chandra et al. (2016) measured the CO_2 and CO mole fractions at Ahmedabad in western India and detected a decrease in the mole fraction when the air mass comes from southwest (ocean) and an increase in the mole fraction when the air mass comes from northeast (inland). Tiwari et al. (2014) analyzed the spatial variability of atmospheric CO_2 mole fractions using models over the Indian subcontinent and began the flask sampling at Sinhagad in western Ghats. They showed (1) the seasonal variation of the CO_2 mole fraction in southern India differed with the variation on the Indo-Gangetic Plain in northern India due to the differences in air mass transportation and anthropogenic activity; (2) the CO_2 mole fraction in July–October at Sinhagad was lower than the mole fraction of CRI on the west coast India because of the influence of photosynthesis by the regional forest ecosystem.

Sreenivas et al. (2016) measured the mole fractions of CO_2 and CH_4 at Shadnagar in central India and reported that the CO_2 and CH_4 mole fractions were strongly positively correlated to anthropogenic sources. Lin et al. (2015) commenced the most ambitious flask sampling network, with sites at Pondicherry (PON) on the southeast coast India, Port Blair (PBL) on Andaman Island, and Hanle (HLE) in northwestern Himalaya. They reported that (1) the mole fractions of CH_4, CO, and N_2O at PON and PBL were relatively high in comparison with those at HLE; (2) seasonal variations in GHGs at PON and PBL were quite different from the variation at HLE because the former two sites were exposed to the influence of air masses originating from areas of anthropogenic activities. In addition to these studies at ground sites, recently aircraft-base

observations over Indo-Gangetic Plain such as CONTRAIL have been also carried out actively, evaluating seasonal variation of CO_2 mole fraction (Umezawa et al, 2016).

Thus, the GHGs observation program in Indian region is expanding gradually, however, the characterization of GHGs behaviour in the northern Indian subcontinent and their long-term trends are not well understood. In this paper, we present the longer GHGs data than previous studies in the Indo-Gangetic Plain including Bangladesh, which is a blank area for GHGs observation and clarify the characteristics of GHGs in the Indian subcontinent by analyzing the periodicity of GHGs growth rates and comparing them with regional climatic conditions. We, therefore, analyzed 14-year record of various GHGs mole fraction and isotopic ratios of CO_2 ($\delta^{13}C$-CO_2 and $\delta^{18}O$-CO_2) at Nainital, India on a mountain site near the Himalayan mountain range, which can be considered as a background site representing Northern Indian air, and which is partly influenced by anthropogenic activities from the Indo-Gangetic Plain. We also show a similar 8-year GHG record at Comilla, Bangladesh located in the eastern edge of Indo-Gangetic Plain, where agricultural activities are believed to be the main factors for GHG emissions. The levels and seasonal variabilities of GHGs mole fraction at these sites are discussed compared to those at other Indian sites reported previously, along with the local precipitation and 72 hr back trajectory to summarize the behavior of GHGs in this region. Relationship of mole fractions among GHGs are evaluated. We also describe isotopic characteristics of CO_2 to consider contribution on absorption by C_3 and C_4 plants in each region. Furthermore, we analyze the relationships between the interannual variabilities in GHG growth rates and regional climatic condition such as the Indian Dipole Mode Index (DMI) and the El Niño Southern Oscillation (ENSO) index.

2 Methods

2.1 Location

Figure 1 shows the locations of Nainital station (NTL) and Comilla station (CLA) where we performed weekly sampling. The GHG observation sites in previous studies on the Indian subcontinent are also marked.

NTL is located at Aryabhatta Research Institute of Observational Sciences (ARIES) (29.36°N, 79.46°E, 1940 m a.s.l.) on the top of Mt. Manora Peak on the foot of the Himalaya mountain range facing the Indo-Gangetic Plain. Also, NTL is located 3 km south of Nainital city and no local residential building within 2 km from the station. Predominant wind direction at NTL show the west-northwest during winter and east during summer (Naja et al., 2016), which mean that the air of NTL is influenced mainly by the air mass passing through the Indo-Gangetic Plain, rather than extremely influenced by local GHGs emissions nearby.

CLA is located at Comilla weather station of Bangladesh Meteorological Department (BMD) (23.43°N, 91.18°E, 30 m a.s.l.) on the edge of farming village with a flat landscape in central Bangladesh. The surrounding area of CLA cover the paddy fields and a few farmhouses. The land use in the Central Bangladesh region is almost exclusively agricultural land, with the structure of farms developing along the roads. Farmers in this region often burn the biomass (e.g. harvest residuals, firewood and dung) and it was expected that CO_2, CH_4, CO, H_2 and N_2O were emitted by the burning. Wind and precipitation are strongly influenced by monsoon and sometimes cyclone hits this region. Wind speeds around the CLA are not very slow on average (e.g., 2-5 m/sec). Therefore, we judged that this site can mainly capture the typical greenhouse gas emission and sink effects in central Bangladesh, which is located in the eastern Indo-Gangetic Plain, despite that it may partly capture some effect from nearby emissions.

2.2 Air sampling

Flask samples were collected from September 2006 in NTL and from June 2012 in CLA. Inlets were mounted at 7 m above ground level (on the roof of the second floor of the station) in NTL and 8 m above ground level (on top of the 5 m tower on the roof of the one-storey weather station building) in CLA. The height of the inlet of NTL is 5-20 m higher than the height

of the canopy close to the inlet. Air samples were collected once a week (usually on Wednesdays) at 2:00 p.m. local time into a 1.5 L Pyrex flask with two stopcocks sealed with Viton O-rings via a sampling line (Figure 2[a]). The sampling line contained a diaphragm pump (MOA-P108-HB, GAST Co., Ltd.) and a freezer (VA-120, Taitec Co., Ltd.) for dehumidification by a glass trap. The sampling flow rate was approximately 2 L min^{-1} and the sample was passed through a -30 °C cooler and pressurized to 0.25 MPa after 10 min flushing through the sampling tube and flask. The sampled flasks were packed in a cardboard box and transported to the laboratory of the Center for Global Environmental Research (CGER), National Institute for Environmental studies, Japan (NIES) (transportation period: 3–7 days) for analyses.

2.3 Measurement methods

Air sample was passed through a -80 °C cold trap for dehumidification and was delivered to each instrument with a flow rate of 40 ml/min (see the analysis line in Fig. 2[b]). A nondispersive infrared analyser (NDIR; LI-COR, LI-6252) was used for CO_2 analysis, a gas chromatograph equipped with a flame ionization detector (GC-FID; Agilent Technologies, HP-5890 or HP-7890) was used to analyze CH_4, a gas chromatograph with a reduction gas detector (GC-RGD; Agilent Technologies, HP-5890+Trace Analytical RGD-2 or Peak Laboratories, Peak Performer 1 RCP) was used for CO and H_2 analyses, and a gas chromatograph with an electron capture detector (GC-ECD) until 2011 and with a micro electron capture detector (GC-micro-ECD) from 2012 (Agilent Technologies, HP-6890) were used to analyze N_2O and SF_6.

Sample was injected to the analytical system three times per one flask and the working standard gases were analyzed after every two flasks. Dry-air mole fractions were measured against each of their working standard gases which were calibrated with NIES secondary standard gas series (CO_2-NIES09 scale, CH_4-NIES94 scale, CO-NIES09 scale, H_2-NIES96 scale, N_2O-NIES01 scale, and SF_6-NIES01 scale). Comparison between those scales and the National Oceanic and Atmospheric Administration (NOAA) scale in the 6th Round Robin intercomparison (NOAA/ESRL, 2019a) showed -0.04 to -0.09 ppm for CO_2, 3.7 to 4.1 ppb for CH_4, 4.0 to 4.4 ppb for CO, -0.61 to -0.69 ppb for N_2O, and -0.03 to -0.06 ppt for SF_6. We evaluated that the NIES scales were almost the same as NOAA scales except for CH_4 which showed a bias that was beyond the measurement precision of our instrument.

The mole fractions of respective working standard gases are 379.00, 403.01, 423.84 and 441.10 ppm for CO_2, 1681.50, 1852.12, 1998.83 and 2167.63 ppb for CH_4, 59.84, 164.57, 267.33 and 373.54 ppb for CO, 401.40, 502,98, 610.49, 715.95 ppb for H_2, 319.23, 326.91, 337.53 and 345.54 ppb for N_2O and 4.65, 9.77, 14.53 and 19.08 ppt for SF_6. Analytical precision for repetitive measurements is less than 0.03 ppm for CO_2, 1.7 ppb for CH_4, 0.3 ppb for CO, 3.1 ppb for H_2, 0.3 ppb for N_2O, and 0.3 ppt for SF_6 (Machida et al., 2008).

After the mole fraction analysis, we used the remaining air inside the flask for analysis of $\delta^{13}C$-CO_2 and $\delta^{18}O$-CO_2. The air was introduced into two traps sequentially (-100 °C and -197 °C), which trapped H_2O and CO_2, respectively. Finally, CO_2 was sealed in a glass tube. Air $\delta^{13}C$-CO_2 and $\delta^{18}O$-CO_2 were measured by MT-252 using the working standard CO_2 gas which was prepared in our laboratory. The method for producing the working standard gas is similar to the method for producing the NIES Atmospheric Reference CO_2 for Isotopic Studies (NARCIS), which is used for interlaboratory-scale comparison (Mukai, 2001). The working standard scales of $\delta^{13}C$-CO_2 and $\delta^{18}O$-CO_2 are the same as those of NARCIS, which were measured by various institutions related to the World Meteorological Organization (WMO) (Mukai, 2003). The differences between NIES scales and INSTAAR (Institute of Arctic and Alpine Research) scales were 0.013–0.039‰ in the mean value range of -8.683 to -8.759‰ for $\delta^{13}C$-CO_2, and -0.017–0.022‰ in the mean value range of -1.956 to -9.299‰ of $\delta^{18}O$-CO_2 in the 6th Round Robin intercomparison (NOAA/ESRL, 2019a). The $\delta^{18}O$-CO_2 for atmospheric CO_2 in this study is expressed against the value of CO_2 evolved from VPDB calcite (i.e., VPDB-CO_2 scale, [IAEA, 1993, Brand et al., 2010]). Although the VSMOW scale is often used for $\delta^{18}O$ values of water, CO_2 evolved from VPDB calcite (VPDB-CO_2 scale) has similar $\delta^{18}O$ values of CO_2 equilibrated with VSMOW water, which is the reference gas of the VSMOW scale. The difference between them is only

0.263‰ (IAEA, 1993, Kim et al., 2015). Additionally, corrections for N_2O bias and $\delta^{17}O$-CO_2 showed by Brand et al. (2010) were made to obtain final isotope ratios.

2.4 Reference dataset

For comparison with the data of NTL and CLA, we obtained weekly data (CO_2, CH_4, CO, N_2O, SF_6, $\delta^{13}C$-CO_2, and $\delta^{18}O$-CO_2) from the Mauna Loa Observatory (MLO) (19.54°N, 155.58°W, 3397 m a.s.l.) on the NOAA/ESRL website (NOAA/ESRL, 2019b). We also used biweekly data for CO_2, CH_4, CO, H_2, N_2O, and $\delta^{13}C$-CO_2 from Cape Rama, India (CRI) (15.08°N, 73.83°W, 60 m a.s.l.) on the website of World Data Centre for Greenhouse Gases (WDCGG) (WDCGG, 2017). The trends of mole fractions of CO_2, CH_4, CO, H_2, N_2O, and SF_6 and the isotopic ratio of $\delta^{13}C$-CO_2 and $\delta^{18}O$-CO_2 were calculated according to the method of Thoning et al. (1989) with a cut-off frequency of 667 days (0.5472 cycles yr^{-1}) for a Fast Fourier Transform (FFT) filter. We also obtained the DMI and ENSO Index from the NOAA/ESRL website (NOAA/ESRL, 2021a; 2021b).

2.5 Weather data

Monthly precipitation data for Nainital uses the monthly precipitation of the state of Uttarakhand, which includes Nainital. The data during January 2007 to December 2019 were taken from the rainfall report on the IMD (India Meteorological Department) website (http://hydro.imd.gov.in/hydrometweb/(S(fqu5hsvtq3sitn45rjia4qma))/landing.aspx). Monthly precipitation data for Comilla uses the average monthly precipitation of Eastern Indo-Gangetic Plain in Bangladesh (Dhaka (23.77°N, 90.38°E and 8 m a.s.l.), Rangpur (25.73°N, 89.23°E and 33 m a.s.l.), Sylhet (24.90°N, 91.88°E and 34 m a.s.l.), Bogra (24.84°N, 89.37°E and 18 m a.s.l.), Ishurdi (24.13°N, 89.05°E and 13 m a.s.l.), Jessore (23.18°N, 89.17°E and 6 m a.s.l.), Feni (23.03°N, 91.42°E and 6 m a.s.l.), Barisal (22.75°N, 90.37°E and 3 m a.s.l.), Chattoogram (22.27°N, 91.82°E and 4 m a.s.l.), and Cox's Bazar (21.43°N, 91.93°E and 2 m a.s.l.)). Data during January 2012 to July 2021 were taken from the JMA (Japan Meteorological Agency) website (http://www.data.jma.go.jp/gmd/cpd/monitor/climatview/frame.php?y=2019&m=7&d=30&e=0).

2.6 Back trajectory analysis

To determine the sources of regional air masses affecting the stations (NTL and CLA), we calculated backward air trajectories using the Meteorological Data Explorer (METEX) system (Zeng and Fujinuma, 2004) available via the website of the Center for Global Environmental Research, National Institute for Environmental Studies (http://db.cger.nies.go.jp/metex/index.html). METEX uses three-dimensional wind speed (horizontal and vertical wind) estimated from the European Centre for Medium Range Weather Forecast (ECMWF) analyses on a 0.5° × 0.5° mesh to calculate 72-h trajectories. We use 1940m for NTL and 30m for CLA as the starting height. We referred the altitude data when we evaluated the effects of GHGs emissions sources near the surface.

The ratio of air mass from south per year was calculated by the frequency of the air mass from south side of Indian Ocean on the flask sampling date in each year with reference to the 72-h backward air trajectories data calculated by METEX.

2.7 Data analysis method for short-term and long-term

Mean values for every 10 days were calculated from the weekly data and were used to calculate the long-term trend and smoothing fitting curve. Because sampling interval is not punctual and we sometimes had missing data, we decided to use 10 days average to calculate the trend curve. The value of the missing period was supplemented with an interpolated values from the previous and following data of the missing period for calculating the continuous long-term trend and smoothing fitting curve.

Long-term trends of the mole fractions were calculated based on the idea of Thoning et al. (1989) with a cut-off frequency of 667 days (0.5472 cycles yr^{-1}) for a FFT filter. The smoothing fitting curve was made for an FFT filter with a cut-off frequency of 50 days (7.3 cycles yr^{-1}).

We defined and expressed seasonal component by a "Δ" term (e.g., ΔCO_2) which was calculated by subtraction of the long-term trend curve from 10 days mean of real data. Also, we defined and expressed short-term variations by a "d" term (e.g., dCO_2), which were characterized by the deviation of 10 days mean of real data from the smoothing fitting curve. Figure 2(c) shows how such components were calculated. Growth rates of mole fraction of observed gases were calculated using the long-term trends.

3. Results and discussion

3.1 Overview of GHGs mole fractions at both sites

Basically, the air masses over the Indian subcontinent were transported from the Indian Ocean region during summer (monsoon season) and from the inland during winter. Air mass trajectories are shown for our sampling sites and related sites in Figure 3. In the case of anthropogenic GHGs, except CO_2, their mole fractions at CLA generally showed relatively low values when the air mass came from the ocean, while the mole fractions were relatively high when the air mass came from inland. On the other hand, mole fractions of GHGs at NTL overall did not show relatively low values, even if the air mass came from the Indian Ocean region (i.e., south-eastern wind) because the air mass from Indian Ocean was strongly affected by local GHGs emissions while passing over the Indo-Gangetic Plain. However, the CO_2 mole fraction changed not only due to transport but also due to the photosynthetic sink strength of terrestrial ecosystems and cultivated crops.

Annual mean GHG mole fractions at NTL and CLA are summarized in Table 1. Annual CO_2 mole fractions at both sites were quite low compared to MLO and other Indian sites such as CRI. For example, in 2010, 386.5 ppm was reported at NTL, 391.9 ppm at CRI (Bhattacharya et al., 2009), and 391.3 ppm was reported at PON (Lin et al. 2015). Note that there is no data for CLA in 2010, however the annual CO_2 mole fraction at CLA is usually only 1–2 ppm higher than at NTL. This seemed to be due to the influence of photosynthesis at both sites. Generally, the CO_2 mole fractions at NTL and CLA decreased strongly (typically twice a year) due to photosynthesis of local crops, making the annual CO_2 mole fractions lower than at other sites despite the likelihood that anthropogenic emission are high in this area.

On the other hand, the annual mean mole fractions of CH_4, CO, H_2, and N_2O at NTL and CLA (Table 1) were almost at the highest levels on the Indian subcontinent due to the influence of strong emission sources. For example, the annual mole fractions of NTL and CLA were 50–470 ppb for CH_4, 30–200 ppb for CO, and 0–5 ppb for N_2O higher compared to other Indian sites (e.g., CRI [Bhattacharya et al., 2009], HLE, PON, and PBL [Lin et al., 2015]). In this region, high CH_4 and N_2O emissions were possible from paddy fields and cultivated areas. Also, much CO is considered to be produced by biomass burning in this region. As for H_2, the mole fraction at CLA was higher than those at other Indian sites, however, it was relatively low at NTL compared to other sites such as CRI (Bhattacharya et al., 2009), PON, and PBL (Lin et al., 2015), but similar to HLE, which is located on a higher mountain. In the case of the SF_6 mole fraction, it has smaller regional differences, suggesting there are no remarkable SF_6 sources near the measurement sites. Below we describe in detail the characteristics of sources and sinks of each component (CO_2, $\delta^{13}C$-CO_2, $\delta^{18}O$-CO_2 CH_4, CO, H_2, N_2O, and SF_6) at NTL and CLA on the Indo-Gangetic Plain in terms of seasonal variations, amplitudes, and growth rates.

3.2 CO_2 and $\delta^{13}C$-CO_2

3.2.1 CO_2 mole fraction and growth rate variations

Figure 4 shows the time series of the atmospheric CO_2 mole fraction and the isotopic ratio of $\delta^{13}C$-CO_2 at our sampling sites (NTL and CLA) together with data from CRI on the west coast of India and MLO in Hawaii. The CO_2 mole fractions at

NTL and CLA in August–October were characteristically lower (approximate 10–20 ppm) than the mole fractions observed at CRI and MLO. The CRI and MLO sites are representative of CO_2 mole fractions in the Southern and Northern Hemisphere, respectively, for the period of the southwest monsoon season (June–September). On the other hand, the $\delta^{13}C$-CO_2 at NTL and CLA were inversely correlated with the CO_2 mole fractions, and generally the values at both sites were higher than at MLO and CRI.

Air masses at NTL and CLA in August–October passed over the Indo-Gangetic Plain and the southeast area of India, respectively, while the air masses of CRI were transported from the Indian Ocean region (Fig. 3). Thus, it was suggested that the air mass from the Indian Ocean in August–October prevailing over CRI was hardly influenced by anthropogenic emission and photosynthesis over the Indian subcontinent, whereas CO_2 mole fractions over NTL and CLA seemed to be influenced during these season by the sources and sinks on the Indo-Gangetic Plain and the south/east areas of the Indian subcontinent. Such transport characteristics must affect the annual average and growth rates in the CO_2 molar ratio and $\delta^{13}C$-CO_2 in addition to their seasonal variations.

We show the CO_2 growth rates observed at NTL, CLA, and MLO in Figure 5(a). Mean CO_2 growth rate at NTL (approximately 2.1 ppm yr^{-1} during 2007–2020) and CLA (approximately 2.9 ppm yr^{-1} during 2013–2020) were similar to other sites (e.g., MLO). However, variations of the calculated growth rates were greater than those at MLO. The range was 0–5 ppm yr^{-1} in the case of NTL, and CLA had higher variability than NTL because local sink and source influences affected the concentration more than remote sites such as MLO. In general, Pacific sites such as MLO and Japanese remote sites in the Northern Hemisphere showed a relationship between CO_2 growth rates and the ENSO index (e.g., Keeling, 1998). This relationship is often explained from the viewpoint of a global temperature anomaly, which has a strong relationship with the ENSO index. On the other hand, the variability at NTL has no associations with the variability in the CO_2 growth rate at MLO and the ENSO index (Fig. 5[b]). Both growth rates seemed to be slightly inversely correlated with each other from 2007 to 2015. However, since then, similar relatively high growth rates have been observed for both sites around 2015-2016 and 2018-2019, indicating that overall, the CO_2 growth rate at NTL is less correlated with the CO_2 growth rate at MLO and the ENSO index.

It is well known that the Indian Ocean Dipole controls meteorological conditions such as air mass transportation and precipitation patterns on the Indian subcontinent (e.g., Saji et al., 1999, Ashok et al., 2004, Hong et al., 2008). Such changes in regional climatic pattern could affect the CO_2 uptake flux by plants in the surrounding area and the atmospheric movement, leading to a change in the CO_2 growth rate. However, we did not find a simple relationship between DMI and CO_2 growth rate at NTL (Fig. 5[b]). Here we have shown that the pattern of CO_2 growth rate in this region is different from the global pattern seen in places like MLO, but the relationship between local climatic factors and changes in CO_2 sinks and emissions is likely to be complex, and further study is needed to interpret the differences.

3.2.2 Seasonal variation and its characteristics

Figure 6(a)-(d) show the seasonal variations in CO_2 mole fractions and isotopic ratios of $\delta^{13}C$-CO_2 at NTL, CLA, CRI, and MLO, which were calculated by subtraction of the measured value from the long-term trend. The annual amplitudes of the CO_2 mole fraction (Table 2) at NTL (22.1 ± 3.9 ppm) and CLA (20.3 ± 5.7 ppm) were much larger than those at other Indian sites (CRI, 15 ppm; HLE, 8.2 ppm; PON, 7.6 ppm; PBL, 11.1 ppm). Also, the annual amplitudes of $\delta^{13}C$-CO_2 at NTL (0.96 ± 0.16‰) and CLA (0.85 ± 0.19‰) were larger than that at CRI (approximately 0.6‰). These results suggested that the atmospheric CO_2 mole fraction of NTL and CLA were strongly influenced by photosynthesis of local plants in summer and their respiration in winter, and other anthropogenic emission which were moderated at the other sites by the influence of the oceanic air. Also, small episodic peaks of the atmospheric CO_2 mole fraction and isotopic ratio of $\delta^{13}C$-CO_2 of CLA at the beginning of each year was influenced by the biomass burning for heating in the close region, which is considered to be inland area from the site according to the air trajectory analysis.

As shown in Figure 4 (a) and (b) and Figure 6(b) and (d), the seasonal variation pattern at CLA has two lower seasons in CO_2 and two higher seasons in $\delta^{13}C$-CO_2 in February–April and July–October. Similarly, in the case of NTL, we sometimes observed relatively low mole fractions of CO_2 in February–March and September, and higher $\delta^{13}C$-CO_2. In general, in many cases including at MLO, only a summer minimum CO_2 mole fraction is observed, while a minimum in February–March is not usually observed.

Twice-yearly decreases in the CO_2 mole fraction have also been observed at several Indian sites such as Dehradun (northern Indian site; Sharma et al., 2013), Sinhagad (western Ghats site; Tiwari et al., 2014), Ahmedabad (western Indian site; Chandra et al., 2016), Shadnagar (central Indian site; Sreenivas et al., 2016), and PON (southeast coast Indian site; Lin et al., 2015), however, these studies did not clearly mention such variations. Umezawa et al. (2016) reported that the decrease in the CO_2 mole fraction near the ground in February–March was caused by photosynthesis of local crops, which was detected by the vertical CO_2 profiles over New Delhi airport. Those sites are located on the Indo-Gangetic Plain or received air masses passing over the Indo-Gangetic Plain or Indian subcontinent. On the other hand, the decrease in the CO_2 mole fraction in February–March was not detected at CRI (west coast Indian site; Bhattacharya et al., 2009), HLE (northwestern Himalayan site), or PBL (Andaman Island's site) (Lin et al., 2015). These sites are not located on the Indo-Gangetic Plain. Thus, air masses at these sites must be mainly transported from the ocean or from areas other than the Indian subcontinent during these periods.

The characteristic CO_2 seasonal variation on the Indo-Gangetic Plain (including NTL and CLA) is very likely to be related to CO_2 uptake by regional vegetation. Generally, in the case of Uttar Pradesh state located in the center of the Indo-Gangetic Plain, rice and other summer plants (maize, millets, etc.) are planted mainly in June–July and harvested in October–November, while large areas of wheat are sown in October–December and harvested in March–April. Therefore, relatively low CO_2 mole fractions observed in those periods are considered to be due to CO_2 uptake by plants cultivated in each season near NTL.

In Bangladesh, rice, being the staple food, is cultivated three times a year in some regions. Usually rice is grown twice (*Aus* and *Amon* rice) from April–October (including the monsoon season), however, often rice is also cultivated (*Boro* rice) in the winter season from November–April (SID/MP, 2018). Other agricultural products include maize, jute, and vegetables in the summer season, and small amount of wheat in the winter season. Therefore, we concluded that the observed lower CO_2 mole fractions in July–October and February–March were influenced by CO_2 uptake by local plants (mainly rice). Especially at CLA, the lower mole fraction in February–March was clear and a strong contribution from CO_2 uptake from *Boro* rice was estimated. As another viewpoint on CO_2 seasonal variation, we observed that the CO_2 maximum in May was not so high, while the CO_2 mole fraction in December was higher. Because precipitation in Bangladesh is stronger than in the north Indian region, the duration of rice cultivation over summertime is also longer than in north India. Therefore, the contribution of plant uptake to the CO_2 mole fraction in the atmosphere at CLA over the summer season is likely to be relatively large compared to that at NTL.

Thus, the decreases in the CO_2 mole fractions in February–March and September in NTL and CLA were estimated to be caused by photosynthesis of plants cultivated in each season over the Indo-Gangetic Plain. NTL and CLA indicated this more clearly compared with other Indian sites due to the proximity to the source region. Figure 7(a) shows the relationships between the annual mean CO_2 mole fraction and $\delta^{13}C$-CO_2 in 2010 and 2012. The slope between the CO_2 mole fraction and $\delta^{13}C$-CO_2 showed -0.050 and -0.054‰ ppm^{-1} which indicated that the spatial variability of the atmospheric CO_2 mole fraction (e.g., a lower mole fraction at NTL than at MLO and CRI) basically occurred due to CO_2 exchange between the atmosphere and terrestrial biosphere.

Furthermore, we examined the relationship of the CO_2 mole fraction and carbon isotope ratio, because there are some seasonal differences in the species cultivation. On the Indo-Gangetic Plain, rice (especially in Bangladesh) and wheat (especially in North India), as C_3 plants, are cultivated in January–March, while C_4 plants (e.g., maize, sugarcane, sorghum

and Bajra (Pearl millet) in addition to rice are cultivated on the Indo-Gangetic Plain and in Bangladesh in June–September (DAC/MA, 2015; SID/MP, 2018; DES/MAFW, 2019). We calculated the end member of the isotope value for absorbed CO_2 by using intercept values of the "Keeling plot" between the reciprocal of the CO_2 mole fraction and the ratio of $\delta^{13}C$-CO_2 obtained from two continuous datasets of air samples, which has > 1 ppm difference in CO_2 mole fraction and > 0.05‰ in $\delta^{13}C$-CO_2. Since in this study two datasets had 1-week intervals, we assumed that the difference in CO_2 and $\delta^{13}C$ between two datasets would include broader influences of photosynthetic activities from relatively large areas on the Indo-Gangetic Plain.

We found that the intercept values of NTL and CLA showed differences in January–March and June–September (Fig. 7[b]), which appeared to reflect the differences in the contributions of C_3 and C_4 plants in this region. In June–September, we found relatively heavier intercept values at both NTL (-25.0 ± 2.4‰) and CLA (-23.5 ± 4.1‰), suggesting that C_4 plants partly contributed to the CO_2 absorption (or emission) in this season, while in January–March, the end member showed -29.0 ± 4.3‰ (NTL) and -28.3 ± 4.0‰ (CLA), which were similar to the general C_3 plant (rice or wheat). If we assume the value for C_4 plant to be -12 to -14‰, the contributions of C_4 plant in NTL and CLA were approximately 25 ± 5% and 31 ± 9%, respectively. According to database (DAC/MA, 2015; SID/MP, 2018; DES/MAFW, 2019) for crops area in Uttar Pradesh district, the area's ratio of C_4 plants (e.g., maize and sugarcane) to C_3 plants in the summer season was approximately 26% in 2012, which was a similar proportion as estimated by the C isotope ratio. In the case of Bangladesh, despite there being no recent data reported, according to data in 2008, the area for maize was approximately < 10% compared to the rice area. However, based on the recent C isotope ratio, it appears likely that more maize has been cultivated.

3.3 $\delta^{18}O$-CO_2

In general, $\delta^{18}O$-CO_2 is related to that value of water in plants and soil, because oxygen atom of CO_2 can be exchanged with oxygen atom of H_2O in plant and bacteria cells during photosynthesis and soil respiration. Plants and soil water mainly originate from rainwater in the study region, however, in the case of the agricultural area, water is often introduced by irrigation systems using river and groundwater. In many cases, photosynthesis produced relatively heavier $\delta^{18}O$-CO_2 than soil respiration because $\delta^{18}O$-H_2O in plant becomes heavier than soil water due to plant transpiration.

Larger amplitudes (approximately 3‰) in the seasonal variation of $\delta^{18}O$-CO_2 at both NTL and CLA were observed, compared to that of MLO (approximately 0.4‰) (Fig. 8[a]). The isotopic ratio of $\delta^{18}O$-CO_2 at CRI (Bhattacharya et al., 2009) was reported to have similar seasonal variation (i.e., high in winter [November–February] and low in September) to our sites. In the Pacific sites like MLO, $\delta^{18}O$-CO_2 has a maximum peak from spring to summer when photosynthesis activity become dominant, while a minimum is seen around fall when the contribution of soil respiration exceeds that of photosynthesis. On the other hand, Indian subcontinent sites seemed to have fairly different seasonal variation patterns, having a maximum in January–February, gradually decreasing from March–September/October, and subsequently rapidly increasing (Fig. 8[c] and [d]). Such seasonal variation may be influenced by photosynthesis and soil respiration in these regions. However, because many crops are cultivated through the year in these areas (as mentioned in section 3.2), the contribution of photosynthesis to the seasonal variation may be relatively small. High soil respiration activity in the wet season can contribute a little more than during the dry season.

On the other hand, seasonal variations in $\delta^{18}O$ of rainwater itself seemed to affect $\delta^{18}O$-CO_2 through photosynthesis and respiration processes. For example, Sengupta and Sarkar (2006) showed the $\delta^{18}O$-H_2O in rain at New Delhi (western Indo-Gangetic Plain) had a higher value in March–May and a minimum value in September. Such variation was fairly consistent with the seasonal variation in $\delta^{18}O$ of CO_2 at NTL. Similarly, CLA has a minimum $\delta^{18}O$-CO_2 in the atmosphere in October, which was the same month in which the minimum $\delta^{18}O$-H_2O was observed in rain in Eastern Indo-Gangetic Plain areas (e.g., Kolkata [near Bangladesh; Sengupta and Sarkar, 2006] and Cherrapunij [Eastern Indo-Gangetic Plain; Breitenbach et al., 2010]). During the rainy season, due to the so-called "amount effect", $\delta^{18}O$-H_2O in rain will decrease with an increase in the amount of precipitation (e.g., Rozanski et al., 1993). However, in the Indian region it has been reported that seasonal changes

in the origin of moisture strongly affected the $\delta^{18}O\text{-}H_2O$ (Sengupta and Sarkar, 2006, Tanoue et al., 2018). In winter (i.e., when there is less rain), moisture comes from the west or north. Therefore, the northern area of the Arabian Sea and the western land area supply moisture, which has a higher $\delta^{18}O\text{-}H_2O$. However, the air mass in the summer monsoon season (mainly June–September) comes from the southern part of the Arabian Sea and sometimes passes over the Bay of Bengal carrying much moisture. The value of $\delta^{18}O\text{-}H_2O$ in the moisture in the air mass decreases with the process of raining along the air trajectory. In the post-monsoon season (mainly October–December), some portion of moisture comes from the Pacific, Bay of Bengal, and the inland area (Tanoue et al., 2018).

In the winter monsoon season (mainly February–May), $\delta^{18}O\text{-}H_2O$ in rain was reported to be approximately 0–1‰ (vs VSMOW). During the winter monsoon season, there is little precipitation, so plant cultivation utilizes irrigation systems using river and groundwater. River and groundwater usually show not so large seasonal variation in $\delta^{18}O$ and have a close value to the annual mean of $\delta^{18}O\text{-}H_2O$ in rain, such as -6 to -8‰ (Kumar et al., 2019). According to the variation of $\delta^{18}O\text{-}CO_2$, in winter its value was approximately 2‰ (vs VPDB-CO_2; VPDB-CO_2 scale is fairly close to the scale of CO_2 equilibrated with VSMOW water as mentioned in section 2.3), which was higher than that of rain and other water reservoirs, suggesting that $\delta^{18}O\text{-}H_2O$ in plants and soil must become higher due to transpiration during dry and relatively warm conditions in winter.

Based on the fact that during the summer monsoon season, $\delta^{18}O\text{-}CO_2$ decreased from 1 to -2‰ with a decrease of $\delta^{18}O\text{-}H_2O$ from 0 to -10 or -15‰ in the rain, the range of variation in $\delta^{18}O\text{-}CO_2$ was approximately one third or one fifth that of rain. Because land water may come from both rain and irrigation systems, the real ranges of $\delta^{18}O$ in soil water and plant water are likely to be smaller than in the case of rain only. Furthermore, because CO_2 from soil respiration contributes more in the rainy season, a balance between photosynthesis and respiration CO_2 will, in general, have a small effect on the seasonal variation.

As for the annual trend of $\delta^{18}O\text{-}CO_2$ shown in Figure 8(b), NTL showed a similar pattern to that of MLO whereas CLA showed a different trend. The $\delta^{18}O\text{-}CO_2$ at NTL began at 0.8‰ in 2007, decreased to 0.2‰ in 2011, then again became heavier (toward 1.0‰) during 2014–2016 (Fig. 8[b]). In northern India, relatively high precipitation was reported during 2011–2013. The tendency of lower $\delta^{18}O\text{-}CO_2$ may have some relationship with the amount of precipitation. In 2008 and 2016 considerable amounts of precipitation fell near NTL. The $\delta^{18}O\text{-}CO_2$ level also seemed to become relatively low. A La Nina event occurred from late 2010 to 2012 and the amount of precipitation increased worldwide from 2010 to 2013. Such large-scale climatic effects are very likely to affect the $\delta^{18}O\text{-}CO_2$ level observed at MLO. In the case of CLA, precipitation increased in 2015–2017 and 2019-2020 (rather than in 2011–2013) and the $\delta^{18}O\text{-}CO_2$ level at CLA seemed to become lower at that time with the increase of precipitation. Analyzing the relationship between the monthly amount of precipitation and $\delta^{18}O\text{-}CO_2$ in Figure 8(e) and (f), a weak negative correlation can be seen (if the monthly mean $\delta^{18}O\text{-}CO_2$ at CLA adds one or two months of time lag to the monthly mean of the precipitation, the correlation coefficient (R^2) between the monthly mean $\delta^{18}O\text{-}CO_2$ at CLA and the monthly mean of precipitation increased to be 0.4 or 0.5). Therefore, the amount of precipitation partly contributes to the regional level of $\delta^{18}O\text{-}CO_2$. However, it must be influenced not only by precipitation but also by seasonal changes in air flow patterns and rain systems, as explained above, as well as by the water reservoir situation, soil water content at that time, and photosynthesis in the region.

If the ground water storage decreases due to wider usage of irrigation and/or less precipitation in recent times, it causes a stronger transpiration effect in the soil environment, making the $\delta^{18}O$ of soil water heavier than usual. Roxy et al. (2015) and Asoka et al. (2017) reported that precipitation over the Indian subcontinent and groundwater storage in northern India has had a decreasing trend due to Indian Ocean warming, which is estimated to have occurred due to the weakening trend of the summer monsoon cross-equatorial flow (Swapna et al., 2014). However, much longer records of CO_2 isotopic ratios are needed to clarify the increasing trend in $\delta^{18}O\text{-}CO_2$ and the relationship with climatic changes in this region.

3.4 CH_4

The CH_4 mole fractions at NTL and CLA are illustrated in Figure 9(a). We detected high CH_4 mole fractions at NTL and CLA, where they sometimes exceeded 2,100 and 4,000 ppb, respectively, showing that the Indo-Gangetic Plain region had relatively strong CH_4 emissions. The seasonal amplitude of the CH_4 mole fraction, especially at CLA (486 ± 225 ppb; Table 2) was much larger than the those of other Indian sites such as NTL (114 ppb), CRI (200 ppb) (Bhattacharya et al., 2009), Darjeeling (400 ppb) (Ganesan et al., 2013), HLE (29 ppb), PON (124 ppb), and PBL (144 ppb) (Lin et al., 2015), which indicated that the contribution of the CH_4 source (e.g., rice cultivation) around CLA was relative strong.

Mean seasonal variations in the CH_4 mole fraction for both sites were calculated and are shown in Figure 9(c) and (d). The mole fractions at both NTL and CLA had the highest peak in August–October and a small peak in March. In general, the CH_4 mole fraction in the Northern Hemisphere decreased in July–September (summer season) through the decomposition process by reaction with OH radicals during this period. A higher CH_4 mole fraction in this period strongly suggests that there are some sources of CH_4. Observation results at Darjeeling (north-eastern Indian site; Ganesan et al., 2013), HLE (Lin et al., 2015), and Shadnagar (Sreenivas et al., 2016) also indicated high CH_4 mole fractions during August–October. Ganesan et al. (2013) reported that the CH_4 mole fraction at Darjeeling was enhanced by transported air masses from the Indo-Gangetic Plain. Lin et al. (2015) and Sreenivas et al. (2016) showed that the high CH_4 mole fractions at HLE and Shadnagar were influenced by emissions from paddy fields and wetlands. Garg et al. (2011) showed that CH_4 emission from rice fields was estimated to be approximately 17% of the total CH_4 emissions in India. According to the emission database of EDGAR v4.3.2 (EC-JRC/PBL, 2016), rice cultivation was the largest source of CH_4 (approximately 50%) in Bangladesh.

Bhatia et al. (2011) measured the CH_4 flux from paddy fields at New Delhi and showed that it was the highest in August–September due to the increase in the activity of rice roots and bacteria in the paddy field soils. Ali et al. (2012) also measured the CH_4 flux from paddy fields at Bangladesh and reported that the CH_4 flux was maximized within 77–98 days after the planting of rice due to the increase in root respiration and carbon in soil. It was considered that both March and September–October were consistent with the timing of increasing CH_4 production at rice fields according to the customary cultivation schedule of rice in this region. In Bangladesh and the eastern Indian district, rice is cultivated from November–September, as mentioned above in the CO_2 section, and CH_4 emissions are considered to continue during winter, supporting higher CH_4 mole fractions from August–March, especially at CLA.

On the other hand, CRI (Bhattacharya et al., 2009), PON, and PBL (Lin et al., 2015) did not show higher CH_4 mole fractions in August–October, as shown in Figure 9(c) and (d). The air masses at those sites in August–October were transported from the Indian Ocean, which may have only a minimal influence from agricultural emission.

CH_4 mole fractions at NTL and CLA were higher than that at MLO, even at the time of year when rice is not cultivated. CH_4 emissions from the enteric fermentation and wastewater handling were reported to be large sources according to the emission database in EDGAR v4.3.2 (EC-JRC/PBL, 2016). Garg et al. (2011) reported that enteric fermentation by cattle and buffalo contributes approximately 40% emissions in India. Such CH_4 emissions must always elevate the CH_4 mole fraction in the air mass in these sites regardless of the season.

In addition, biomass burning (including residential cooking and agricultural residue burning) is very likely to have contribution to the CH_4 mole fraction according to the inventory evaluation (i.e., 21% contribution; Garg et al, 2011). Reasonably good correlations were seen between short term components in variations of CH_4 and CO in January–March, April–June, and October–December. Ratios of dCH_4 to dCO showed ranges such as 0.64–0.80 ppb ppb^{-1} in NTL and 1.85–1.98 ppb ppb^{-1} in CLA, as shown in Figure. 9(e) and (f). One of the major CO sources in India was considered to be biomass burning (Dickerson et al., 2002). Akagi et al (2011), EC-JRC/PBL (2016), and Sfez et al. (2017) reported that the emission ratios of CH_4 to CO in biomass burning such as crop residue burning, firewood burning, and biogas burning were 0.04–0.90 ppb ppb^{-1}. Therefore, the ratios observed in these seasons could suggest a strong influence on CH_4 and CO emissions from

biomass burning (such as crop residue burning), despite the other large CH_4 emissions such as paddy fields and waste treatment, which will increase the ratio, especially at CLA in July–September.

As a result, it is evident that annual CH_4 mole fractions at the sites used in this study on the Indo-Gangetic Plain are enriched by various CH_4 sources, depending on the season. Generally speaking, because April–June is a dry and hot season, CH_4 decomposition processes will proceed, decreasing its mole fraction at both sites.

The variability in the CH_4 growth rate in the trend line at NTL was different to the variability at MLO (Fig. 9[b]), which may be influenced by regional climatic condition, including the Indian Ocean Dipole. Because the frequency of air mass transportation from the south increased if the Indian Ocean Dipole was often activated, the air mass passed over the Indo-Gangetic Plain (which has strong CH_4 emissions), reaching NTL with a high CH_4 mole fraction. The difference between the variability in the CH_4 growth rate between NTL and CLA may also be explained by the above hypothesis. If the frequency of air mass transportation from the south increased by the activation of Indian Ocean Dipole (e.g., in 2015) because the air mass was directly transported from the Indian Ocean with a relatively low CH_4 mole fraction, the CH_4 mole fraction at CLA would become relatively low compared to a usual year (Fig. 9[b]). On the other hand, as mentioned previously, in 2015–2017, even in high Indian Ocean Dipole mode, Bangladesh had relatively high precipitation which could strengthen CH_4 production from rice paddy fields and other aquatic environments. This potential situation well-matched the high CH_4 mole fraction in summer and the high growth rate at CLA during 2016–2017.

3.5 CO

High annual CO mole fractions at both NTL and CLA (Table 1) indicated that the atmosphere over the Indo-Gangetic Plain was influenced by strong CO emission sources such as burning of harvest residues and residential burning using solid biofuel, which are considered to be main CO emission sources in the region (EC-JRC/PBL, 2016). However, of course, CO originating from car exhaust and industrial activities remains very likely to have made some contributions to the CO mole fraction (EC-JRC/PBL, 2016).

The main crops around NTL are rice and wheat and the harvesting periods are September–November and April–May, respectively (DAC/MA, 2015). Farmers in this area generally burn harvest residues at their farmland after harvest (Lohan et al., 2018). Venkataraman et al. (2006) reported that the amount of burning on the Western Indo-Gangetic Plain has two peaks annually, i.e., in May and November. We could observe the same seasonal variation in the CO mole fraction in the atmosphere at NTL (Fig. 10[c]). Kumar et al. (2011) also reported that the highest densities in fire spots were seen in spring and autumn on the western Indo-Gangetic Plain. These suggested that CO emissions from the burning of harvest residues was one of the most important sources on the Western Indo-Gangetic Plain in these seasons.

On the other hand, the seasonal variation in CO mole fraction at CLA exhibited only one peak in October–March (Fig. 10[d]). Such seasonal variation was also detected at CRI (Bhattacharya et al., 2009), PON, PBL (Lin et al., 2015), and Ahmedabad (Chandra et al., 2016). In Bangladesh, after the end of the monsoon (October–March), harvest residues are burnt and used to make bricks using some kinds of biofuel as a heat source (Guttikunda et al., 2012). Also, dung is burnt for the stove (Venkataraman et al., 2010) during the winter season. In addition, biofuel is used for cooking (Lawrence and Lelieveld, 2010) throughout the year. Those activities could emit large amounts of CO (Streets et al., 2003; Venkataraman et al., 2010; Maithel et al., 2012).

In addition, the seasonal amplitude of the CO mole fraction (Table 2) at CLA (356 ± 90 ppb) on the Eastern Indo-Gangetic Plain site was much larger than that observed in other Indian sites (e.g., CRI [200 ppb], PON [78 ppb], PBL [144 ppb], and Ahmedabad [270 ppb]). The highest CO amplitude observed at CLA was consistent with the model estimation of CO emissions, which showed that the Eastern Indo-Gangetic Plain included areas with the highest CO emissions (Kumar et al., 2013).

On the other hand, the annual mean CO mole fraction at NTL gradually decreased approximately by 50 ppb for 10 years (2006–2015; Fig. 10[a]). Especially, the monthly mean CO mole fraction in November of each year (i.e., the highest level in the year) at NTL decreased by 120 ppb during that period. This suggests that the amount of harvest residues burnt decreased, the ratio of incomplete combustion in car engines was improved, or the type of fossil fuel for cooking changed from biofuel to natural gas. Such decreasing trends in the CO mole fraction level were also detected by Pandey et al. (2017) who reported total-column CO levels during 2003–2014 over the Indo-Gangetic Plain. However, the CO mole fraction level at NTL appeared to increase slightly from 2015. Although the reason for the increase is unclear from this study only, CO emissions from car exhaust were recently estimated to have increased (EC-JRC/PBL, 2016). Therefore, further monitoring is important.

The trend in the CO mole fraction and its inter-annual variability at NTL was similar to those in CH_4 at NTL (Fig. 9[b] and Fig. 10[b]). The mole fractions of CO and CH_4 at NTL tended to be slightly higher when the air mass passed over the Indo-Gangetic Plain, where there are strong sources of both CO and CH_4. In 2015 and 2017, a large positive Indian Dipole Mode occurred, in addition to El Nino in 2015. Therefore, we observed more frequent southern winds, causing higher CH_4 and CO mole fractions at NTL. However, at CLA, southern wind will decrease the mole fraction of CO. Thus, temporal variations of both CO and CH_4 mole fractions in both sites must be strongly controlled by meteorological conditions as well as source strength.

3.6 H_2

Mole fractions, growth rates, and seasonal variations of H_2 at both sites are shown in Figure 11(a-d). It was found that CLA, especially, showed a higher mole fraction than the other sites. Novelli et al. (1999) reported that the main sources of H_2 were combustion (fossil fuel combustion and biomass burning) and photochemical sources such as the oxidation of CH_4 and non-CH_4 hydrocarbons (NMHCs), which account for 90% of the total source. The other 10% is attributed to emissions from volcanoes, oceans, and nitrogen fixation by legumes. Therefore, we have to assume that there are some emission sources at CLA.

On the other hand, H_2 is removed from the troposphere by reacting with OH and by deposition and oxidation at surface soil. The amounts of sources and sinks for H_2 in the global budget were estimated to be equal, resulting in a near-equilibrium state (Novelli et al., 1999). The strengths of H_2 removal in the atmosphere over the Indian subcontinent do not differ greatly by region according to Yashiro et al. (2011), whereas the strengths of H_2 sources may differ by region (Price et al., 2007). Lin et al. (2015) reported that H_2 mole fractions at Indian sites were influenced by biomass burning and were 0–40 ppb higher than those at regional background sites (e.g., eastern Kazakhstan and central China). Figure 11(c) and (d) show the seasonal variations of the H_2 mole fraction at NTL and CLA, which illustrate the maximum in May and the minimum in December at NTL, and the maximum in November–January and the minimum in June–August at CLA, which were different from the averaged seasonal variation in the Northern Hemisphere, which showed the maximum in March–April and the minimum in August–September (Novelli et al., 1999).

Because the burning of biomass (such as harvest residuals and dung) appeared to be actively carried out on the Indo-Gangetic Plain (including at NTL) during April–May and at CLA during November–February, H_2 production must, therefore, increase during these seasons. Furthermore, since higher CH_4 mole fractions at NTL and CLA were observed during August–September and September–October due to strong paddy field emissions at those times, H_2 production from CH_4 degradation can also increase. Figure 11(e) and (f) show short-term variable components (such as dCO and dH_2, and dCH_4, and dH_2) at both NTL and CLA during those periods, and that they had positive correlations. These figures may suggest some relationship between H_2 emission with biomass burning, and between photochemical reactions between OH and CH_4, respectively. Furthermore, the minimum H_2 in June–August was influenced by a fresh air mass from the Indian Ocean which is only minimally affected by anthropogenic emission.

As mentioned above, the H_2 mole fraction level at CLA was higher than that at NTL. The amplitude of the seasonal variation of the H_2 mole fraction (Table 2) at CLA showed 70.4 ± 42.2 ppb, which was also larger than the amplitudes at other Indian sites such as Nainital (50 ppb), CRI (50 ppb) (Bhattacharya et al., 2009), HLE (22 ppb), PON (16 ppb), and PBL (22 ppb) (Lin et al., 2015). These tendencies were consistent with the results of Price et al. (2007), which indicated a larger H_2 emission area around the Eastern Indo-Gangetic Plain, such as at CLA, than on the Western Indian subcontinent. Thus, our observation and previous studies both indicated that the Indian subcontinent had relatively strong H_2 sources.

3.7 N_2O

Garg et al. (2012) reported that the agricultural sector accounted for approximately 75% of the total N_2O emission in India in 2005, including around 49% from nitrogen fertilizer use. In particular, they reported that northern India (the Indo-Gangetic Plain) has the highest N_2O emission in India because nitrogen fertilizer was applied to extensive paddy fields, was denitrified, and N_2O was produced and emitted to the atmosphere. Ganesan et al. (2013) reported that the N_2O mole fraction at Darjeeling (north-eastern Indian site) was enhanced due to air mass transportation from the Indo-Gangetic Plain. The annual mean N_2O mole fraction at NTL (Table 1) appeared to be almost the same as at Darjeeling sites in North India and was higher than at another two Indian sites (CRI [Bhattacharya et al., 2009] and HLE [Lin et al., 2015]) and at MLO (Fig. 12[a]).

Thompson et al. (2014) estimated that the N_2O emissions of the Eastern Indo-Gangetic Plain, including CLA, were higher than those of the Western Indo-Gangetic Plain. This is supported by our observation results that show that the N_2O annual mean mole fraction during 2013–2019 at CLA on the Eastern Indo-Gangetic Plain was 1–2 ppb higher than at NTL on the Western Indo-Gangetic Plain (Table 1), and the seasonal amplitude of the N_2O mole fraction (Table 2) at CLA (4.25 ± 1.45 ppb) was higher than the amplitudes at other Indian sites (NTL, CRI [Bhattacharya et al., 2009], HLE, PON, and PBL [Lin et al., 2015]). Raut et al. (2011) reported the highest N_2O emission rates in the regions of Bangladesh and Sri Lanka due to their high usage of urea as a fertilizer.

However, interestingly, PON and PBL, where oceanic air from the Bay of Bengal affected the sites (Lin et al, 2015) seemed to have relatively higher mole fractions than the sites in this study. As for the seasonal variation in the N_2O mole fraction at NTL, a higher mole fraction was seen in May–September (Fig. 12[c]). Generally, nitrogen fertilizer was frequently applied to paddy fields in May–September in northern India. Gupta et al. (2016) measured the N_2O flux in paddy fields at New Delhi and reported that the flux increased immediately after the application of nitrogen fertilizer to the fields. Therefore, high N_2O levels and increases in the N_2O mole fraction at NTL in May–September were influenced by the enhancement of the N_2O flux due to the denitrification of nitrogen fertilizer in paddy fields.

The N_2O mole fraction at CLA increased in November–February (Fig. 12[d]) and such seasonal variation was almost identical to the seasonal variation in CO at CLA. The seasonal component in the N_2O mole fraction (ΔN_2O = deviation of N_2O mole fraction from the long-term trend) at CLA showed positive correlations (R^2 = 0.81–0.88) with that of the CO mole fraction (ΔCO) each year (Fig. 11[e]). Also, their ratio ($\Delta N_2O/\Delta CO$) showed 0.013–0.015 ppb ppb^{-1}, which was same (0.015 ppb ppb^{-1}) as the ratio of total N_2O and total CO emissions in Bangladesh from the EDGAR v4.3.2 database (EC-JRC/PBL, 2016). Although such seasonal variation is likely to be partly related to the lower mixing height in the winter season, variations in N_2O emission flux must affect the seasonal variations in the mole fraction. In general, the CO mole fraction was influenced by biomass burning in this season. Because many inventory data showed that biomass burning produced both N_2O and CO, N_2O may be affected partly emitted from biomass burning. However, the emission ratios of N_2O to CO are fairly variable with an approximate range of 0.0004–0.017 (Andreae and Merlet, 2001; Sahai et al., 2007, 2011; EDGAR v4.3.2 [EC-JRC/PBL, 2016]). It seemed that this ratio changes with the type of plants that are burnt. According to Sahai et al. (2011), because the ratio was approximately 0.004 in the case of rice straw, some portion (e.g., 0.004/0.015, i.e., approximately 27% at the most) of N_2O in the atmosphere may originate from biomass burning. In addition, since Venkataraman et al. (2010) reported that dung burning is one of major N_2O sources among many kinds of biomass burning in India, its contribution was also possible.

On the other hand, nitrification and denitrification processes of nitrogen fertilizer in rice paddy soil are considered to be major causes of N_2O emissions in this region (EDGAR v4.3.2), however, the emission rate appeared to have seasonal variation. Related to the irrigation system, the N_2O flux was thought to be larger in alternating wet and dry conditions than under continuously flooded conditions (Akiyama et al., 2005; Gaihre et al., 2018; Begum et al., 2019). In the summer monsoon season, many rice paddies fields in Bangladesh must have enough water level because of the ample amount of precipitation. After the summer monsoon (from October), the water level in the paddy field intermittently changed with the situation. Therefore, relatively a higher N_2O emission rate likely occurred during the winter season, when rice (*Boro* rice) was still grown, enhancing the N_2O mole fraction in the winter season. Further observations of high frequency variations of both N_2O and CO mole fractions will contribute towards precisely evaluating the N_2O emission sources at this site.

The N_2O growth rates at NTL and CLA were similar to that of MLO (Fig. 12[b]), however, the variations in the N_2O growth rate at both NTL and CLA were larger than that of MLO during 2016–2020. The variation in the N_2O growth rate showed a similar pattern to the growth rates of CO and H_2 (Fig. 9[b] and Fig. 10[b]), indicating that the sources of these gases had basically common characteristics.

3.8 SF_6

SF_6 is mainly emitted artificially from factories and urban areas (Olivier et al., 2005). Ganesan et al. (2013) reported that the SF_6 emission at Darjeeling (northeastern Indian site) was considerably weak. Our results also showed that SF_6 mole fractions at NTL and CLA were almost the same as the background SF_6 mole fraction (e.g., MLO in Fig. 13[a] and other sites such as HLE, PON, and PBL [Lin et al., 2015]). In addition, the annual amplitudes of the SF_6 mole fraction at Indian sites (HLE, PON, and PBL) were 0.15, 0.24, and 0.48 ppt, respectively, which were almost within the same range (0.15–0.23 ppt) as at NTL and CLA (Table 2). These results suggested that there was no large SF_6 source on the Indo-Gangetic Plain.

Figure 13(c) and (d) show that the seasonal variations of the SF_6 mole fraction at NTL and CLA decreased in summer (NTL: July, CLA: June–August), which was the same variation as those detected at PON and PBL (Lin et al., 2015). In the summer season, air masses from the south via the Indian Ocean prevailed in the NTL and CLA regions, as shown in Figure 2. Generally, the SF_6 mole fraction in the Southern Hemisphere was lower than that in the Northern Hemisphere (Geller et al., 1997). Thus, the seasonal variation in the SF_6 mole fraction was explained by the frequency of air mass transportation from the south.

Figure 13(b) shows the interannual variability of the SF_6 growth rate at NTL, CLA, and MLO and southern air mass contribution at NTL and CLA. The variability in the SF_6 growth rate at NTL was different to the variability at MLO, and in fact we could see an anticorrelation between them. In the case of CLA, an anticorrelation was not so clear because of a relatively shorter data record. The decrease in the growth rate at NTL seemed to have a relationship with the increase in the frequency of southern air mass transportation. This indicated that the growth rate of the SF_6 mole fraction at NTL may be controlled by the regional climatic condition though the transportation process. Because SF_6 had weaker sources in Northern India, the variation in its trend could be explained more clearly by the influence of the air mass movements.

As mentioned above, anticorrelation in the growth rates between MLO and this region was also seen in CO_2 and CH_4. Therefore, we must take into consideration the influence of the variation in large-scale atmospheric circulation to the GHG mole fraction and trends in their growth rates in the Indian region.

4. Conclusions

We characterized GHGs and related gases over the Northern Indian region using air samples collected weekly at Nainital, India (NTL), and Comilla, Bangladesh (CLA), since 2006 and 2012, respectively. Observation data at both NTL and CLA were compared with the GHG data of other Indian sites and Mauna Loa, Hawaii (MLO) in the Pacific station. From this

comprehensive analysis, it was found that the feature of seasonal and long-term variations in each gas were influenced by the local sinks and sources during each season, and annual climatic conditions on the Indo-Gangetic Plain. They were considerably different to those of the MLO in the Pacific region.

On the Indo-Gangetic Plain, rice, wheat, other cereals, and millet are cultivated in the respective seasons corresponding to the change between wet and dry climatic conditions. Therefore, seasonal variations in the atmospheric CO_2 mole fraction were strongly influenced by the crop CO_2 sink at that time. In general, low CO_2 mole fractions in the winter season in the Northern Hemisphere were not observed, however, we observed relatively lower mole fractions during January–March in this region, especially at CLA. In Bangladesh, rice is grown even in the winter season. The $\delta^{13}C$-CO_2 signature showed C_3 plants (e.g., rice and wheat) affected the CO_2 mole fractions in the winter season, while in the summer season the $\delta^{13}C$-CO_2 signature showed C_4 plants (corn, sugar cane etc.) contributed some portion.

The seasonal variations in $\delta^{18}O$-CO_2 showed almost the same variation as that in the $\delta^{18}O$ in local rain. Effects of the amount of precipitation and the origin of moisture, appeared to affect $\delta^{18}O$ in local rain and CO_2. As a result, $\delta^{18}O$ in CO_2 was affected by the climatic variation related to the amount of precipitation, which was enhanced during 2015–2017. These facts are also consistent with the explanation that CO_2 exchange by photosynthesis (and respiration) by land biomass strongly affected CO_2 seasonality in mole fraction.

At both sites, higher CH_4 mole fractions were observed than were recorded at other Indian sites. Especially, higher mole fractions than 4000 ppb were recorded at CLA, where rice paddy fields covered the area. Rice cultivation was one of major emission sources in this region. Because CH_4 production activities increased after rice planting, we observed the highest peak in September–October at both sites and a small peak in spring at CLA. A large amount of precipitation during those seasons is likely to have affected the CH_4 production rate of rice paddy fields through soil anaerobic conditions and, as a result, increased the atmospheric CH_4 mole fraction. Air mass transport also influenced seasonal variation and the variability of its growth rate. Beside emissions from rice paddy fields, we identified the relationship between biomass burning and the CH_4 mole fraction in a season other than September–October, when biomass burning occurred frequently. In addition, enteric fermentation and wastewater handling were large emission sources in this region. The large number of sources appeared to increase the average CH_4 mole fraction in this region.

CO was strongly related to biomass burning activities at both sites. The mole fraction was high in the dry season and after crop harvesting. At CLA in winter, a higher mole fraction was observed together with a high N_2O mole fraction, which may suggest some link to biomass burning as a N_2O source. The CO level gradually decreased throughout the observed period. CO emissions must, therefore, be reduced by various technical progresses including automobile emission and industrial combustion efficiency improvements.

We observed higher N_2O levels in the crop season (i.e., the rainy season) from May–September at NTL, but much higher levels in the winter season at CLA. N_2O is known to be mainly emitted from soil though nitrogen fertilizer applications to rice fields and crop lands in this region. However, for CLA, we estimated seasonal variations in the emission rate due to the water level in the rice paddy field, because intermittent irrigation in winter generally produces more N_2O than continuously flooded conditions in the rainy season.

H_2 showed some relationship to both CO and CH_4 mole fractions. We found that CO had a good correlation with H_2 in the biomass burning season, indicating some H_2 contribution from biomass burning. On the other hand, in the season when the CH_4 mole fraction was high, the H_2 mole fraction was also relatively high compared to CH_4, suggesting that chemical reactions of CH_4 and H_2 may contribute some portion of the H_2 mole fraction.

SF_6 showed consistent mole fractions with other Indian sites. Seasonal variations were strongly related to the southern air mass frequency, because the SF_6 mole fraction in the southern region was relatively low.

We found that the interannual variabilities in CH_4, SF_6 and also partly in CO_2, growth rates at NTL were anticorrelated with those at MLO, which is located in the Pacific. Growth rates for many GHGs are known to be influenced by El Nino events

for many reasons (e.g., hot climate, dry conditions on a global scale). However, in the Indian region, growth rates of some GHGs seemed to be more affected by the regional climate condition such as the Indian Ocean Dipole, which usually affects air circulation and precipitation in the Indian region. In the case of CLA, although the data duration was insufficiently short, growth rates of CO_2, CH_4, and SF_6 changed differently from those at MLO, which could be partly explained by the climatic variations due to the Indian Ocean Dipole. Because CLA is located relatively close to the ocean, sometimes the variation was thought to be different from that at NTL.

These findings have not been reported previously. In this study, long-term records of GHGs data at NTL enabled a long-term analysis. These findings suggested that the mole fractions of GHGs and their emissions on the Indian subcontinent could change with climatic conditions in this region in the near future, in addition to changes in anthropogenic activities relating to GHG emissions and countermeasure for the emissions. Therefore, long-term GHG monitoring should be continued and the effectiveness of countermeasures for reducing GHG emissions on the Indian subcontinent, including the Indo-Gangetic Plain, should be evaluated.

5. Data availability

We will add digital object identifiers (DOIs) to weekly flask sampling data of Nainital and Comilla and those data on our website (http://db.cger.nies.go.jp/portal/geds/atmosphericAndOceanicMonitoring) by 2021.

Conflicts of Interest

The authors declare no conflicts of interest.

Acknowledgments

We would like to thank Deepak Singh Chausali and other staff of the Aryabhatta Research Institute of Observational Sciences (ARIES), and the staff of Comilla weather station in Bangladesh Meteorological Department (BMD) for their great support in this project. The establishment and running of the air sampling program were partly supported by the Asia Pacific Network (grant ARCP2011-11NMY-Patra/Canadell), and the Environment Research and Technology Development Fund (JPMEERF20152002 and JPMEERF20182002) of the Ministry of the Environment, Japan and the Environmental Restoration and Conservation Agency of Japan. We thank Pieter Tans, Ed. Dlugokencky, Paul. C. Novelli Geoff. Dutton, Bradley Hall and the Earth System Research Laboratory team of the National Oceanic and Atmospheric Administration (NOAA), and James White, Bruce Vaughn and Sylvia Michel and the Institute of Arctic and Alpine Research team of the University of Colorado for providing the data of Mauna Loa Observatory.

References

Akagi, S. K., Yokelson, R. J., Wiedinmyer, C., Alvarado, M. J., Reid, J. S., Karl, T., Crounse, J. D., and Wennberg, P. O.: Emission factors for open and domestic biomass burning for use in atmospheric models. Atmospheric Chemistry and Physics, 11(9), 4039-4072, 2011.

Akiyama, H., Yagi, K., and Yan, X.: Direct N_2O emissions from rice paddy fields: summary of available data. Global Biogeochemical Cycles, 19(1), 2005.

Ali, M. A., Farouque, M. G., Haque, M., and ul Kabir, A.: Influence of soil amendments on mitigating methane emissions and sustaining rice productivity in paddy soil ecosystems of Bangladesh. Journal of Environmental Science and Natural Resources, 5(1), 179-185, 2012.

Andreae, M. O., and Merlet, P.: Emission of trace gases and aerosols from biomass burning. Global biogeochemical cycles, 15(4), 955-966, 2001.

Arino, O., Perez, R. J., Julio, Kalogirou V., Bontemps S., Defourny P., and Van Bogaert E.: Global land cover map for 2009 (GlobCover 2009), European Space Agency (ESA) & Université catholique de Louvain (UCL), 2012. [Available at http://www.esa-landcover-cci.org.]

Ashok, K., Guan, Z., Saji, N. H., and Yamagata, T.: Individual and combined influences of ENSO and the Indian Ocean dipole on the Indian summer monsoon. Journal of Climate, 17(16), 3141-3155, 2004.

Asoka, A., Gleeson, T., Wada, Y., and Mishra, V.: Relative contribution of monsoon precipitation and pumping to changes in groundwater storage in India. Nature Geoscience, 10(2), 109-117, 2017.

Begum, K., Kuhnert, M., Yeluripati, J. B., Ogle, S. M., Parton, W. J., Williams, S. A., Pan, G., Cheng, K., Ali, M. A. and Smith, P.: Modelling greenhouse gas emissions and mitigation potentials in fertilized paddy rice fields in Bangladesh. Geoderma, 341, 206-215, 2019.

Bhatia, A., Ghosh, A., Kumar, V., Tomer, R., Singh, S. D., and Pathak, H.: Effect of elevated tropospheric ozone on methane and nitrous oxide emission from rice soil in north India. Agriculture, ecosystems and environment, 144(1), 21-28, 2011.

Bhattacharya, S. K., Borole, D. V., Francey, R. J., Allison, C. E., Steele, L. P., Krummel, P., Langenfelds, R., Masarie, K. A., Tiwari, Y. K., and Patra, P. K.: Trace gases and CO_2 isotope records from Cabo de Rama, India, Curr. Sci., 97, 1336–1344, 2009.

Brand, W. A., Assonov, S. S., and Coplen, T. B.: Correction for the ^{17}O interference in δ (^{13}C) measurements when analyzing CO_2 with stable isotope mass spectrometry (IUPAC Technical Report). Pure and Applied Chemistry, 82(8), 1719-1733, 2010.

Breitenbach, S. F. M., Adkins, J. F., Meyer, H., Marwan, N., Kumar, K. K., and Haug, G. H.: Strong influence of water vapor source dynamics on stable isotopes in precipitation observed in Southern Meghalaya, NE India, Earth Planet Sci. Lett., 292, 212-220, 2010.

Chandra, N., Lal, S., Venkataramani, S., Patra, P. K., and Sheel, V.: Temporal variations of atmospheric CO_2 and CO at Ahmedabad in western India, Atmos. Chem. Phys., 16, 6153–6173, doi:10.5194/acp-16-6153-2016, 2016.

DAC/MA.: Agricultural Statistics at a Glance 2014, Directorate of Economics and Statistics, Department of Agriculture and Cooperation (DAC), Ministry of Agriculture (MA), Government of India, Oxford Univ. Press, New Delhi, India, 2015.

DES/MAFW.: Crop Production Statistics for Selected States, Crops and Range of Year, Directorate of Economics and Statistics (DES), Ministry of Agriculture and Farmers Welfare (MAFW), Government of India. https://aps.dac.gov.in/APY/Public_Report1.aspx (accessed 2019-July-31), 2019.

Dickerson, R. R., Andreae, M. O., Campos, T., Mayol - Bracero, O. L., Neususs, C., and Streets, D. G.: Analysis of black carbon and carbon monoxide observed over the Indian Ocean: Implications for emissions and photochemistry. Journal of Geophysical Research: Atmospheres, 107(D19), 2002.

EC-JRC/PBL.: EDGAR v4.3.2 (1970 - 2012) on March 2016, Emissions Database for Global Atmospheric Research (EDGAR), European Commission, Joint Research Centre (EC-JRC), Netherlands Environmental Assessment Agency (PBL), http://edgar.jrc.ec.europa.eu, 2016.

Friedlingstein, P., Jones, M. W., O'Sullivan, M., Andrew, R. M., Hauck, J., Peters, G. P., et al.: Global carbon budget 2019, Earth System Science Data, 11(4), 1783–1838. https://doi.org/10.5194/essd-11-1783-2019, 2019.

Gaihre, Y. K., Singh, U., Islam, S. M., Huda, A., Islam, M. R., Sanabria, J., Satter, M. A., Islam, M. R., Biswas, J. C., Jahiruddin, M., and Jahan, M. S.: Nitrous oxide and nitric oxide emissions and nitrogen use efficiency as affected by nitrogen placement in lowland rice fields. Nutrient cycling in agroecosystems, 110(2), 277-291, 2018.

Ganesan, A. L., Chatterjee, A., Prinn, R. G., Harth, C. M., Salameh, P. K., Manning, A. J., Hall, B. D., Mühle, J., Meredith, L. K., Weiss, R. F., O'Doherty, S., and Young, D.: The variability of methane, nitrous oxide and sulfur hexafluoride in Northeast India, Atmos. Chem. Phys., 13, 10633–10644, doi:10.5194/acp-13- 10633-2013, 2013.

Garg, A., Kankal, B., and Shukla, P. R.: Methane emissions in India: Sub-regional and sectoral trends,.Atmospheric Environment, 45(28), 4922-4929, 2011.

Garg, A., Shukla, P. R., and Upadhyay, J.: N_2O emissions of India: an assessment of temporal, regional and sector trends, Clim. Change, 110, 755-782, doi:10.1007/s10584-011-0094-9, 2012

Geller, L. S., Elkins, J. W., Lobert, J. M., Clarke, A. D., Hurst, D. F., Butler, J. H., and Myers, R. C.: Tropospheric SF_6: observed latitudinal distribution and trends, derived emissions and interhemispheric exchange time, Geophys. Res. Lett., 24, 675–678, 1997.

Gupta, D. K., Bhatia, A., Kumar, A., Das, T. K., Jain, N., Tomer, R., Sandeep, k. M., Fagodiya, R. K., Dubey, R., and Pathak, H.: Mitigation of greenhouse gas emission from rice–wheat system of the Indo-Gangetic Plain: Through tillage, irrigation and fertilizer management. Agriculture, Ecosystems and Environment, 230, 1-9, 2016.

Guttikunda, S., Begum, B., and Wadud, Z.: Particulate pollution from brick kiln clusters in the Greater Dhaka region, Bangladesh. Air Quality, Atmosphere and Health, 1e9, 2012.

Hong, C. C., Li, T., and Kug, J. S.: Asymmetry of the Indian Ocean dipole. Part I: observational analysis. Journal of climate, 21(18), 4834-4848, 2008.

IAEA: Reference and comparison materials for light isotopes of light elements, Proceedings of a consultants meeting held in Vienna, IAEA-TECDOC-825,1993

Keeling, C. D.: Rewards and penalties of monitoring the Earth. Annual Review of Energy and the Environment, 23(1), 25-82, 1998.

Kim S. Coplen, T. B. and Horita J.: Normalization of stable isotope data for carbonate minerals: Implementation of IUPAC guidelines. Geochimica et Cosmochimca Acta, 158, 276-289, 2015.

Kumar, A., Sanyal, P., and Agrawal, S.: Spatial distribution of $\delta^{18}O$ values of water in the Ganga river basin: Insight into the hydrological processes, Journal of Hydrology, 571, 225-234, 2019.

Kumar, R., Naja, M., Satheesh, S. K., Ojha, N., Joshi, H., Sarangi, T., Pant, P., Dumka, U. C. Hegde, P. and Venkataramani, S.: Influences of the springtime northern Indian biomass burning over the central Himalayas. Journal of Geophysical Research: Atmospheres, 116(D19), 2011.

Kumar, R., Naja, M., Pfister, G. G., Barth, M. C., and Brasseur, G. P.: Source attribution of carbon monoxide in India and surrounding regions during wintertime. Journal of Geophysical Research: Atmospheres, 118(4), 1981-1995, 2013.

Lawrence, M. G., and Lelieveld, J.: Atmospheric pollutant outflow from southern Asia: a review. Atmospheric Chemistry and Physics, 10(22), 11017, 2010.

Lin, X., Indira, N. K., Ramonet, M., Delmotte, M., Ciais, P., Bhatt, B. C., Reddy, M. V., Angchuk, D., Balakrishnan, S., Jorphail, S., Dorjai, T., Mahey, T. T., Patnaik, S., Begum, M., Brenninkmeijer, C., Durairaj, S., Kirubagaran, R., Schmidt, M., Swathi, P. S., Vinithkumar, N. V., Yver Kwok, C., and Gaur, V. K.: Long-lived atmospheric trace gases measurements in flask samples from three stations in India. Atmos. Chem. Phys., 15, 9819–9849, doi:10.5194/acp-15-9819-2015, 2015.

Lohan, S. K., Jat, H. S., Yadav, A. K., Sidhu, H. S., Jat, M. L., Choudhary, M., Peter, J. D. and Sharma, P. C.: Burning issues of paddy residue management in north-west states of India. Renewable and Sustainable Energy Reviews, 81, 693-706, 2018.

Machida, T., Matsueda, H., Sawa, Y., Nakagawa, Y., Hirotani, K., Kondo, N., Goto, K., Nakazawa, T., Ishikawa, K. and Ogawa T.: Worldwide Measurements of Atmospheric CO_2 and Other Trace Gas Species Using Commercial Airlines. J. Atmos. Ocean. Technol., 25, 1744–1754, doi:10.1175/2008JTECHA1082.1, 2008.

Maithel, S., Uma, R., Bond, T., Baum, E., and Thao, V. T. K.: Brick kilns performance assessment, emissions measurements, and a roadmap for cleaner brick production in India. Study report prepared by Green Knowledge Solutions, New Delhi, 2012.

Mukai H.: NIES pure CO_2 sample for inter-laboratory comparison of C and O isotope ratio analysis especially for atmospheric CO_2, proceeding of the 11th WMO/IAEA Meeting of Experts on Carbon Dioxide Mole fraction and Related Tracer Measurement Techniques. In: WMO/GAW Rep, 31, 2001.

Mukai H.: Inter-Comparison of Isotope Ratios For CO_2 Using Several Reference Materials, proceeding of the 12th WMO/IAEA Meeting of Experts on Carbon Dioxide Mole fraction and Related Tracer Measurement Techniques, In: WMO/GAW Rep, 58–62, 2003.

Naja, M., Bhardwaj, P., Singh, N., Kumar, P., Kumar, R., Ojha, N., ... & Kotamarthi, V. R.: High-frequency vertical profiling of meteorological parameters using AMF1 facility during RAWEX–GVAX at ARIES, Nainital, Corrent Science, 111(1), 132-140, 2016.

NOAA/ESRL.: The 6th WMO/IAEA Round Robin Comparison Experiment. http://www.esrl.noaa.gov/gmd/ccgg/wmorr/wmorr_results.php?rr=rr6&param=co2&group=group5 (accessed 2019-May.-15), 2019a.

NOAA/ESRL.: ESRL/GMD FTP Data Finder. https://www.esrl.noaa.gov/gmd/dv/data/ (accessed 2019-May.-15), 2019b.

NOAA/ESRL.: Dipole Mode Index. https://www.esrl.noaa.gov/psd/gcos_wgsp/Timeseries/DMI/ (accessed 2021a-Apr.-6), 2021.

NOAA/ESRL.: Multivariate ENSO Index. https://www.esrl.noaa.gov/psd/enso/mei/ (accessed 2021-Apr.-6), 2021b.

Novelli, P. C., Lang, P. M., Masarie, K. A., Hurst, D. F., Myers, R., and Elkins, J. W.: Molecular hydrogen in the troposphere: Global distribution and budget, J. Geophys. Res. Atmos., 104, 30427–30444, 1999.

Olivier, J. G. J., Van Aardenne, J. A., Dentener, F., Ganzeveld, L., and Peters J. A. H. W.: Recent trends in global greenhouse gas emissions: regional trends and spatial distribution of key sources, in: Non-CO_2 Greenhouse Gases (NCGG-4), edited by: Van Amstel, A., 325-330, Millpress, Rotterdam, The Netherlands, 2005.

Pandey, A. K., Mishra, A. K., Kumar, R., Berwal, S., Devadas, R., Huete, A., and Kumar, K.: CO variability and its association with household cooking fuels consumption over the Indo-Gangetic Plain. Environmental pollution, *222*, 83-93, 2017.

Patra, P. K., Canadell, J. G., Houghton, R. A., Piao, S. L., Oh, N. H., Ciais, P., Manjunath, K. R., Chhabra, A., Wang, T., Bhattacharya, T., Bousquet, P., Hartman, J., Ito, A., Mayorga, E., Niwa, Y., Raymond, P. A., Sarma, V. V. S. S., and Lasco, R..: The carbon budget of South Asia. Biogeosciences, 10(1), 513-527, 2013.

Price, H., Jaegle, L., Rice, A., Quay, P., Novelli, P. C., and Gammon, R.: Global budget of molecular hydrogen and its deuterium content: Constraints from ground station, cruise, and aircraft observations, J. Geophys. Res., 112, D22108, doi:10.1029/2006JD008152, 2007.

Raut, N., Sitaula, B. K., and Bajracharya, R. M.: Agricultural intensification in South Asia and its contribution to greenhouse gas emission: A review, Asian Jornal of water, environment and pollution, 8(3), 11-17, 2011.

Roxy, M. K., Ritika, K., Terray, P., Murtugudde, R., Ashok, K., and Goswami, B. N.: Drying of Indian subcontinent by rapid Indian Ocean warming and a weakening land-sea thermal gradient, Nature communications, 6, 7423, 2015.

Rozanski, K., Araguás - Araguás, L., and Gonfiantini, R.: Isotopic patterns in modern global precipitation, in *Climate change in continental isotopic records, Geophys. Monogr. Ser.*, vol. 78, edited by P. K. Swart et. al., pp. 1-36, AGU, Washington, D. C., 1993.

Sahai, S., Sharma, C., Singh, D. P., Dixit, C. K., Singh, N., Sharma, P., Singh, K., Bhatt, S., Ghude, S., Gupta, V., Gupta, R. K., Tiwari, M. K., Garg, S. C., Mitra, A. P. and Gupta, R. K.: A study for development of emission factors for trace gases

and carbonaceous particulate species from in situ burning of wheat straw in agricultural fields in India. Atmospheric Environment, 41(39), 9173-9186, 2007.

Sahai, S., Sharma, C., Singh, S.K., and Gupta, P.K.: Assessment of trace gases, carbon and nitrogen emissions from field burning of agricultural residues in India. Nutrient Cycling in Agroecosystems 89, 143e157, 2011.

Saji, N. H., Goswami, B. N., Vinayachandran, P. N., and Yamagata, T.: A dipole mode in the tropical Indian Ocean. Nature, 401(6751), 360, 1999.

Sengupta, S. and Sarkar, A.: Stable isotope evidence of dual (Arabian Sea and Bay of Bengal) vapour sources in monsoonal precipitation over north India. Earth Planet. Sci. Lett. 250, 511–521, 2006.

Sfez, S., De Meester, S., and Dewulf, J.: Co-digestion of rice straw and cow dung to supply cooking fuel and fertilizers in rural India: Impact on human health, resource flows and climate change. Science of the Total Environment, 609, 1600-1615, 2017.

Sharma, N., Nayak, R. K., Dadhwal, V. K., Kant, Y., and Ali, M. M.: Temporal variations of atmospheric CO_2 in Dehradun, India during 2009, Air Soil Water Res., 6, 37–45, 2013.

SID/MP.: Statistical Year Book Bangladesh 2018, Statistics and Informatics Division (SID), Ministry of Planning (MP), Government of the people's republic of Bangladesh, Dhaka, Bangladesh, 2018.

Sreenivas, G., Mahesh, P., Subin, J., Kanchana, A. L., Rao, P. V. N., and Dadhwal, V. K.: Influence of Meteorology and interrelationship with greenhouse gases (CO_2 and CH_4) at a suburban site of India, Atmos. Chem. Phys., 16, 3953–3967. doi:10.5194/acp-16-3953-2016, 2016.

Streets, D. G., Yarber, K. F., Woo, J.-H., and Carmichael, G. R.: Biomass burning in Asia: Annual and seasonal estimates and atmospheric emissions, Global Biogeochem. Cy., 17, 1099, doi:10.1029/2003GB002040, 2003.

Swapna, P., Krishnan, R., and Wallace, J. M.: Indian Ocean and monsoon coupled interactions in a warming environment, Climate dynamics, 42(9-10), 2439-2454, 2014.

Tanoue, M., Ichiyanagi, K., Yoshimura, K., Kiguchi, M., Terao, T., and Hayashi, T.: Seasonal variation in isotopic composition and the origin of precipitation over Bangladesh, Progress in Earth and Planetary Science, 5-77, 2018.

Thompson, R. L., Ishijima, K., Saikawa, E., Corazza, M., Karstens, U., Patra, P. K., Bergamaschi, P., Chevallier, F., Dlugokencky, E., Prinn, R. G., Weiss, R. F., O'Doherty, S., Fraser, P. J., Steele, L. P., Krummel, P. B., Vermeulen, A., Tohjima, Y., Jordan, A., Haszpra, L., Steinbacher, M., Van der Laan, S., Aalto, T., Meinhardt, F., Popa, M. E., Moncrieff, J., and Bousquet, P.: TransCom N_2O model inter-comparison – Part 2: Atmospheric inversion estimates of N_2O emissions, Atmos. Chem. Phys., 14, 6177–6194, doi:10.5194/acp-14-6177-2014, 2014.

Thoning, K.W., Tans, P.P. and Komhyr W.D.: Atmospheric carbon dioxide at Mauna Loa Observatory, 2. Analysis of the NOAA GMCC data, 1974–1985. J. Geophys. Res., 94 (D6), 8549–8565, 1989.

Tiwari, Y. K., Vellore, R. K., Ravi Kumar, K., van der Schoot, M., and Cho, C.-H.: Influence of monsoons on atmospheric CO_2 spatial variability and ground-based monitoring over India, Sci. Total Environ., 490, 570–578, doi:10.1016/j.scitotenv.2014.05.045, 2014.

Umezawa, T., Niwa, Y., Sawa, Y., Machida, T., and Matsueda, H.: Winter crop CO_2 uptake inferred from CONTRAIL measurements over Delhi, India. Geophysical Research Letters, 10.1002/2016GL070939, 11859-11866, 2016.

Venkataraman, C., Habib, G., Kadamba, D., Shrivastava, M., Leon, J. F., Crouzille, B., Boucher, O., and Streets, D. G.: Emissions from open biomass burning in India: Integrating the inventory approach with high - resolution Moderate Resolution Imaging Spectroradiometer (MODIS) active - fire and land cover data. Global biogeochemical cycles, 20(2), 2006.

Venkataraman, C., Sagar, A. D., Habib, G., Lam, N., and Smith, K. R.: The Indian national initiative for advanced biomass cookstoves: the benefits of clean combustion. Energy for Sustainable Development, *14*(2), 63-72, 2010.

WDCGG.: Data/Quick Plot. http://ds.data.jma.go.jp/gmd/wdcgg/cgi-bin/wdcgg/accessdata.cgi?index=CRI215N00-CSIRO&select=inventory (accessed 2017-Dec.-14), 2017.

Yashiro, H., Sudo, K., Yonemura, S., and Takigawa, M.: The impact of soil uptake on the global distribution of molecular hydrogen: chemical transport model simulation. Atmospheric Chemistry and Physics, 11(13), 6701-6719, 2011.

Zeng, J. and Fujinuma, Y.: New web site launched for online air trajectory calculation. EOS, Transactions American Geophysical Union 85(46), 482, 2004.

Tables

Table 1. Annual mean atmospheric mole fractions of CO_2, CH_4, CO, H_2, N_2O, and SF_6, isotopic ratio of $\delta^{13}C$-CO_2 and $\delta^{18}O$-CO_2 and CO_2 growth rate at Nainital (NTL) and Comilla (CLA) in 2007–2020.

Site	Year	CO_2 ppm		CH_4 ppb		CO ppb		H_2 ppb		N_2O ppb		SF_6 ppt		$\delta^{13}C$-CO_2 ‰		$\delta^{18}O$-CO_2 ‰		CO_2 Growth rate	
		Ave	S.D	Ave	S.D	Ave	S.D	Ave	S.D	Ave	S.D	Ave	S.D	Ave	S.D	Ave	S.D	Ave	S.D
Nainital	2007	380.6	9.6	1928.4	70.6	238.7	100.5	546.1	19.7	321.9	0.83	6.25	0.17	-8.14	0.44	0.72	1.09		
Nainital	2008	383.2	7.8	1931.0	75.5	225.4	99.4	551.8	24.1	323.0	0.83	6.57	0.29	-8.15	0.35	0.50	1.00	-0.4	0.95
Nainital	2009	383.5	9.3	1919.4	63.3	210.2	79.2	538.8	28.0	323.7	0.88	6.95	0.28	-8.13	0.44	0.55	0.87	3.3	0.76
Nainital	2010	386.5	9.0	1925.7	59.7	214.4	92.6	537.9	25.6	324.7	0.87	7.19	0.24	-8.19	0.42	0.28	1.13	0.7	0.28
Nainital	2011	389.6	6.3	1945.2	70.3	213.7	72.1	544.6	24.5	325.4	0.97	7.52	0.21	-8.28	0.32	0.35	1.20	2.3	0.78
Nainital	2012	391.2	7.5	1956.0	76.7	222.1	79.3	552.6	29.9	326.2	1.18	7.85	0.35	-8.22	0.33	0.31	1.12	4.1	0.74
Nainital	2013	391.7	8.0	1963.1	58.2	223.2	69.7	549.9	24.8	327.2	1.03	8.11	0.15	-8.19	0.39	0.47	1.29	0.1	0.92
Nainital	2014	394.3	7.5	1961.2	75.4	205.5	66.0	543.0	22.9	328.3	1.17	8.48	0.16	-8.25	0.34	0.92	0.93	1.3	0.76
Nainital	2015	396.0	8.3	1984.1	72.8	226.6	77.1	549.3	28.1	329.4	1.02	8.84	0.23	-8.24	0.38	1.04	0.87	2.3	1.55
Nainital	2016	400.8	8.2	1990.0	62.8	227.6	77.7	557.1	24.1	329.9	0.92	9.05	0.14	-8.36	0.39	0.92	1.10	3.6	1.83
Nainital	2017	401.6	8.5	2012.1	83.8	229.0	77.8	555.9	26.3	331.0	1.24	9.43	0.16	-8.28	0.41	0.90	1.08	2.8	1.00
Nainital	2018	404.3	7.8	2013.8	67.9	225.1	82.8	559.7	33.2	332.2	0.95	9.74	0.14	-8.36	0.36	0.91	1.10	1.4	0.31
Nainital	2019	406.3	8.8	2021.3	64.1	232.4	84.3	556.8	29.5	332.7	1.08	10.10	0.13	-8.36	0.40	0.81	1.19	3.1	0.84
Nainital	2020	407.4	6.7	2037.3	88.2	206.8	75.0	563.8	48.8	334.0	1.32	10.43	0.17	-8.33	0.31	0.66	1.21		
Comilla	2013	393.7	9.0	2214.6	291.6	294.7	168.8	607.7	69.3	328.4	2.29	8.12	0.18	-8.41	0.38	0.42	0.95	4.6	1.73
Comilla	2014	395.4	10.8	2274.0	402.3	318.6	162.2	612.1	53.7	330.0	2.36	8.46	0.16	-8.44	0.45	0.52	0.82	-1.4	0.95
Comilla	2015	395.6	7.2	2272.4	250.6	293.8	118.4	596.0	32.6	330.5	1.87	8.78	0.13	-8.34	0.32	0.44	0.87	5.0	2.70
Comilla	2016	402.4	8.1	2363.3	399.5	292.5	119.9	652.5	81.0	330.9	1.75	9.01	0.16	-8.54	0.35	0.11	1.17	4.2	1.85
Comilla	2017	404.6	8.8	2484.5	450.1	293.4	129.2	601.9	27.6	332.1	2.29	9.37	0.19	-8.54	0.38	-0.14	1.23	1.8	1.79
Comilla	2018	403.8	8.1	2380.0	253.4	295.7	135.4	669.3	85.6	333.0	1.82	9.68	0.10	-8.47	0.34	0.16	0.86	0.5	3.05
Comilla	2019	408.9	7.9	2406.7	331.5	284.5	114.0	604.6	36.9	333.9	1.81	10.07	0.16	-8.58	0.33	-0.06	1.44	5.5	0.90
Comilla	2020	415.2	11.2	2830.6	679.6	339.9	167.4	639.0	91.8	336.0	3.08	10.46	0.24	-8.73	0.50	-0.31	1.15		

Table 2. Mean annual amplitudes of seasonal variation in atmospheric mole fractions of CO_2, CH_4, CO, H_2, N_2O, and SF_6 and $\delta^{13}C\text{-}CO_2$ and $\delta^{18}O\text{-}CO_2$ at Nainital (NTL) during 2007–2019 and at Comilla (CLA) during 2013–2019.

Site	CO_2 ppm	CH_4 ppb	CO ppb	H_2 ppb	N_2O ppb	SF_6 ppt	$\delta^{13}C\text{-}CO_2$ ‰	$\delta^{18}O\text{-}CO_2$ ‰
Nainital	22.1 ± 3.9	114 ± 52	153 ± 44	50.3 ± 18.0	1.01 ± 0.74	0.18 ± 0.16	0.96 ± 0.16	2.71 ± 0.79
Comilla	20.3 ± 5.7	486 ± 225	356 ± 90	70.4 ± 41.2	4.25 ± 1.45	0.23 ± 0.08	0.85 ± 0.19	2.33 ± 0.49

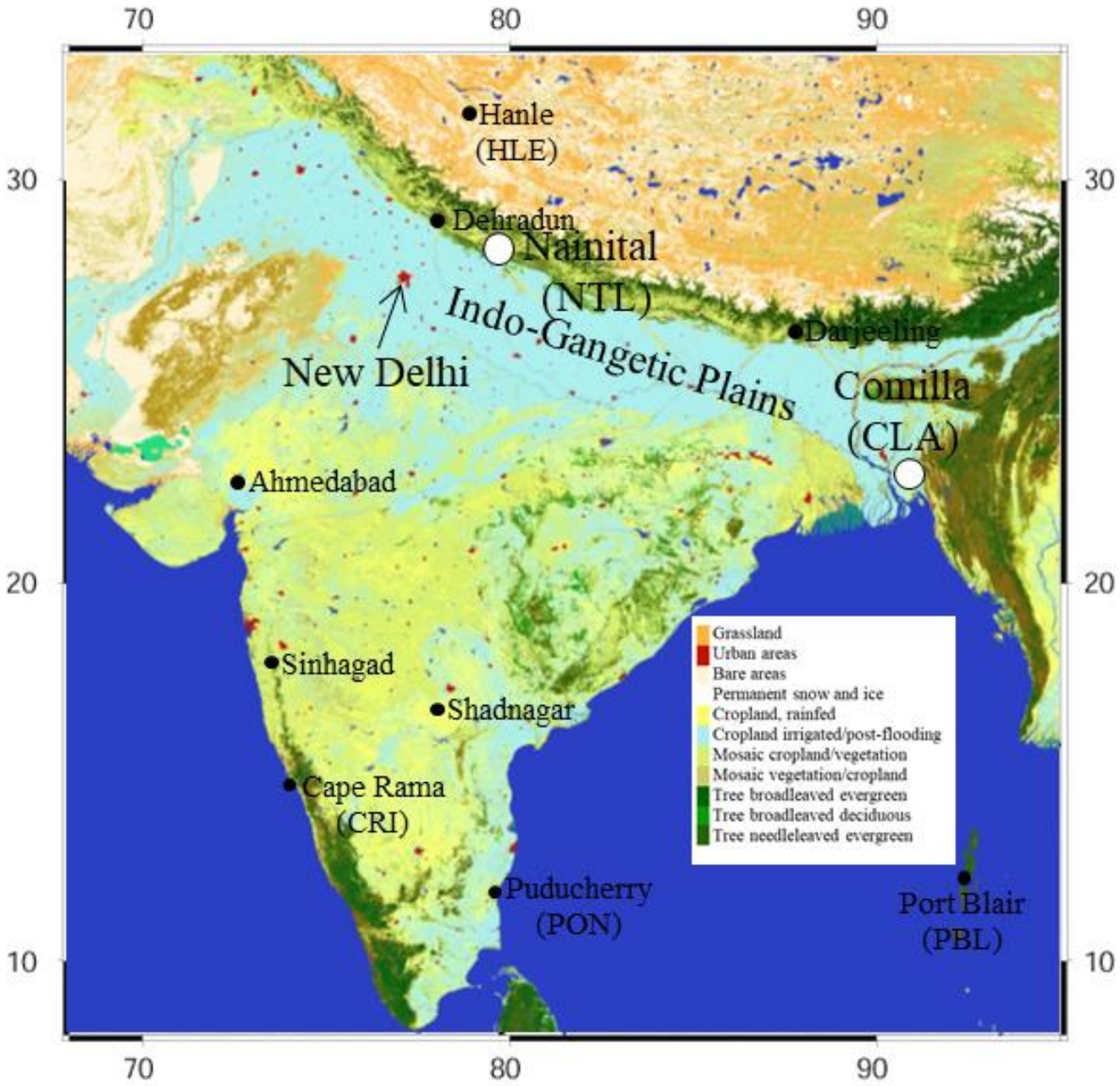

Figure 1. Location of Nainital (NTL), India (29.36°N, 79.46°E, 1940 m a.s.l.) and Comilla (CLA), Bangladesh (23.43°N, 91.18°E, 30 m a.s.l.) and other Indian sites for greenhouse gas (GHG) observation (Bhattacharya et al. 2009; Ganesan et al. 2013; Sharma et al., 2013; Tiwari et al., 2014; Lie et al., 2015; Sreenivas et al., 2016; Chandra et al.; 2016) and showing land cover around the South Asia region (Arino et al., 2012).

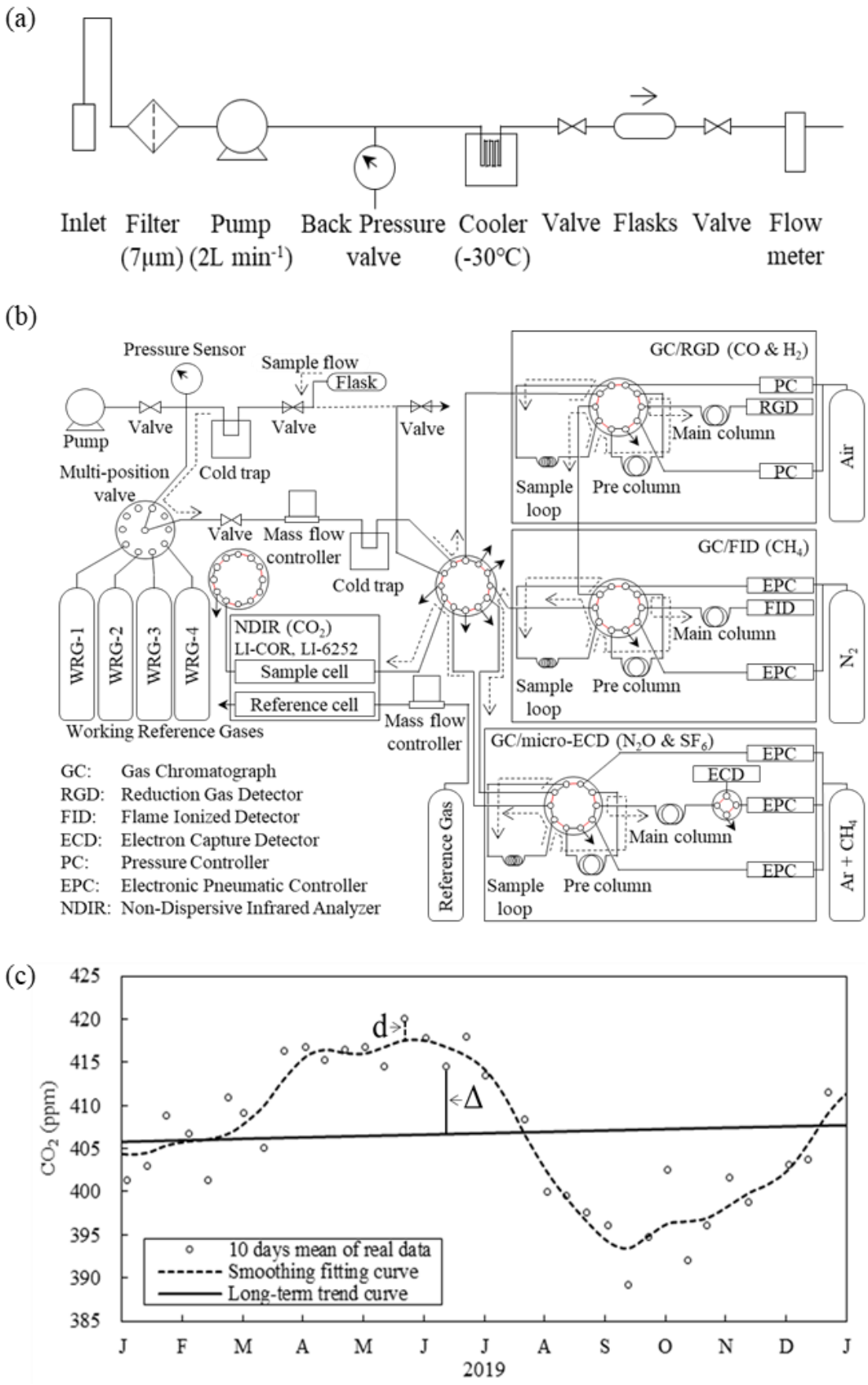

Figure 2. The line used for (a) flask sampling, (b) schematic of measurements of the dry-air mole fraction in the laboratory and (c) diagram of the calculation method for "Δ" term (e.g., ΔCO_2) which was calculated by subtraction of the long-term trend curve from 10 days mean of real data and "d" term (e.g., dCO_2) which was characterized by the deviation of 10 days mean of real data from the smoothing fitting curve.

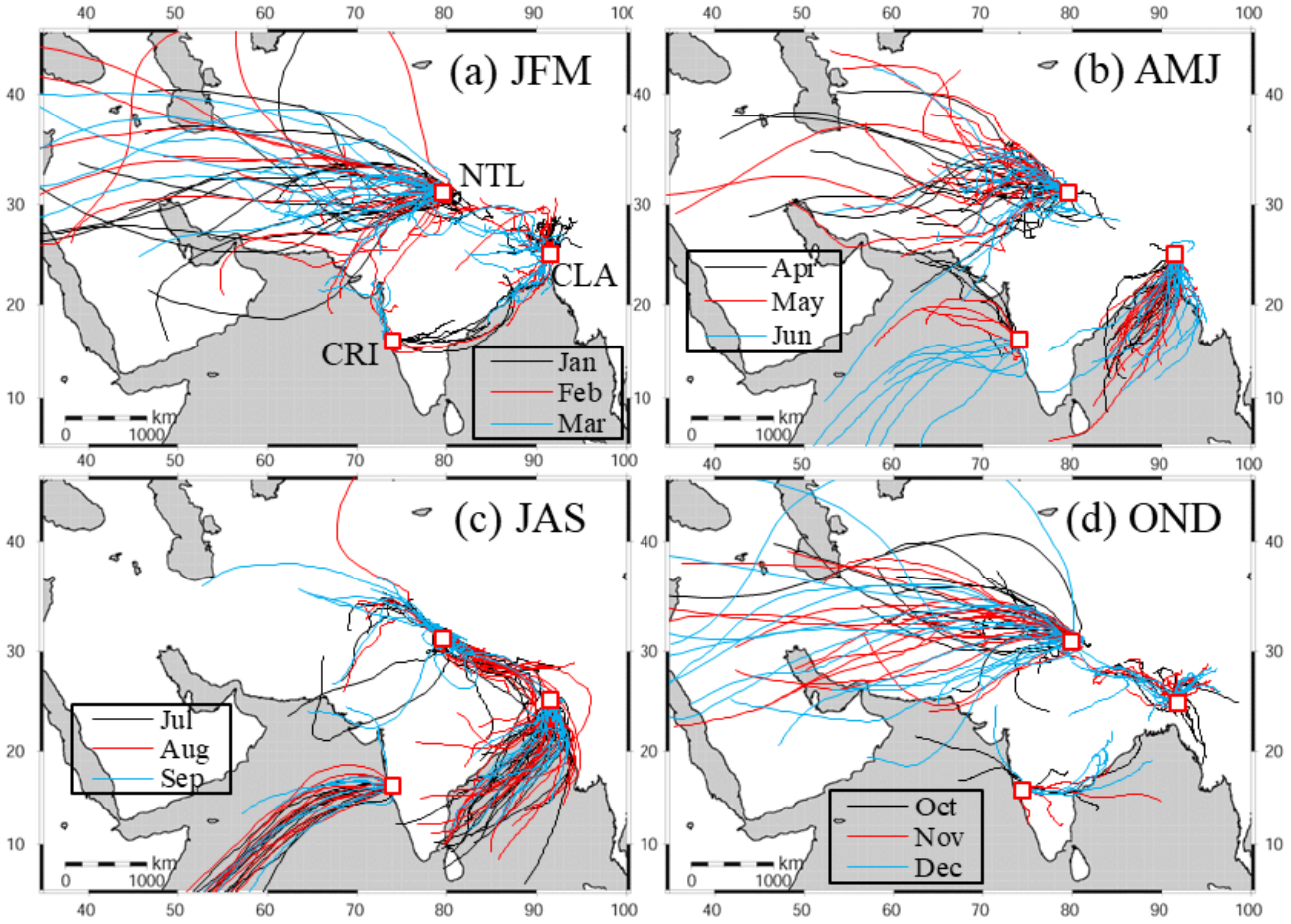

Figure 3. 72-hour back trajectory of Nainital (NTL), Comilla (CLA), and Cape Rama (CRI) in (a) January–March (JFM), (b) April–June (AMJ), (c) July–September (JAS), and (d) October–December. 72-hour back trajectory at NTL and CLA showed for 2012–2016 and the back trajectory at CRI showed for 2009–2013.

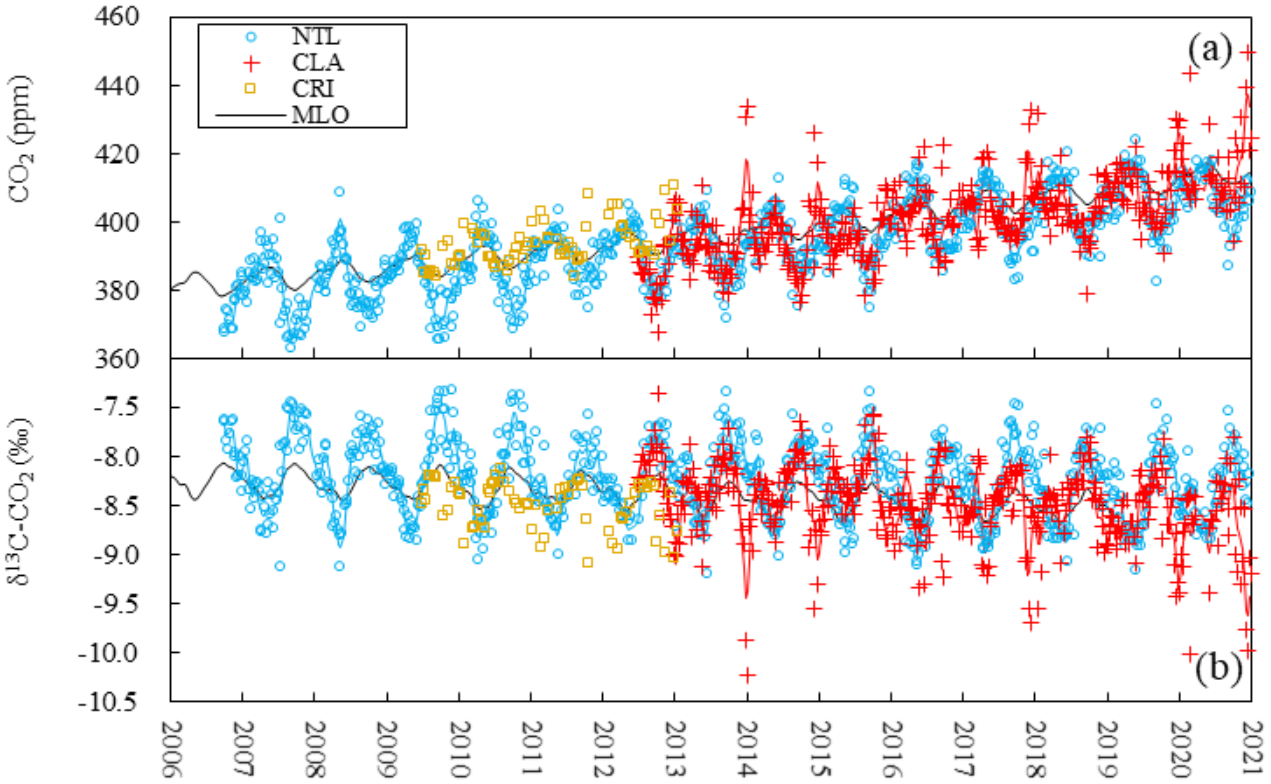

903
904

905 Figure 4. Time series of the (a) atmospheric CO_2 mole fraction, and (b) isotope ratio of $\delta^{13}C$-CO_2 at Nainital (NTL), Comilla
906 (CLA), Cape Rama (CRI), and Mauna Loa (MLO) in 2006–2020.

907
908
909

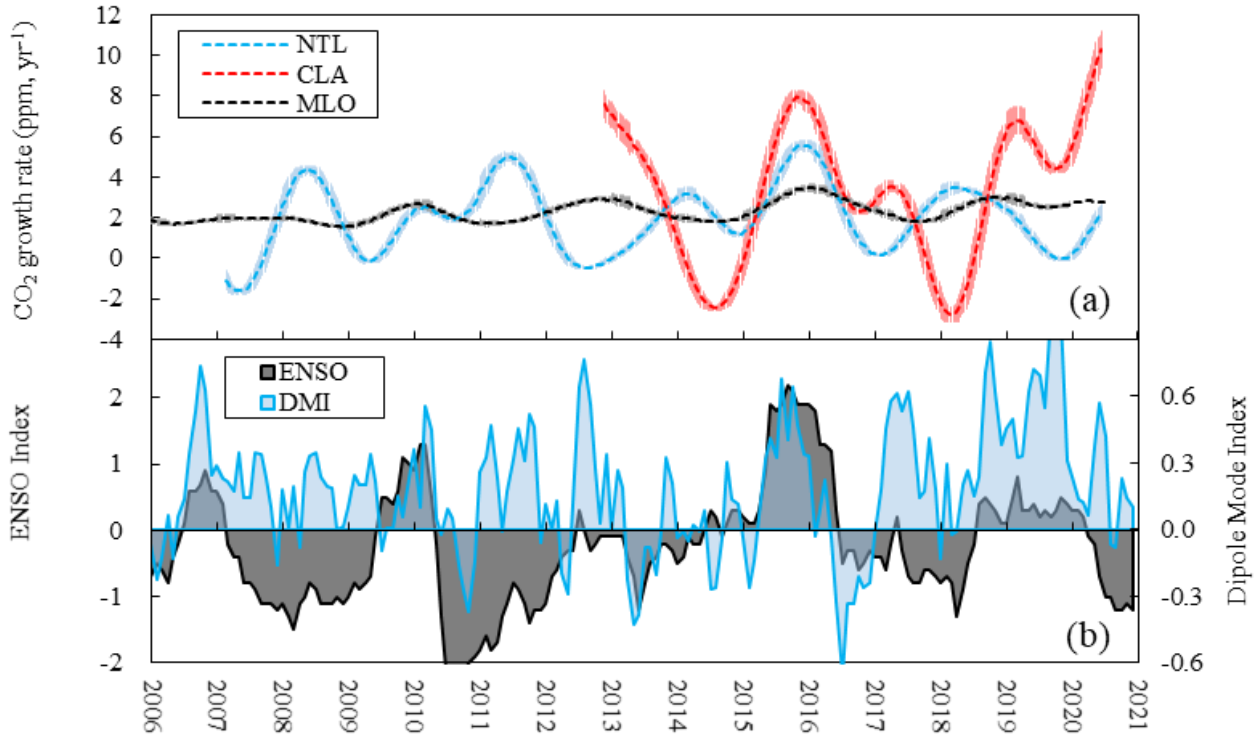

Figure 5. (a) Growth rates of the CO_2 mole fraction at Nainital (NTL), Comilla (CLA), and Mauna Loa (MLO) in 2006–2020, and (b) the El Nino Southern Oscillation (ENSO) Index in 2006–2020 and the Dipole Mode Index (DMI) in 2006–2020.

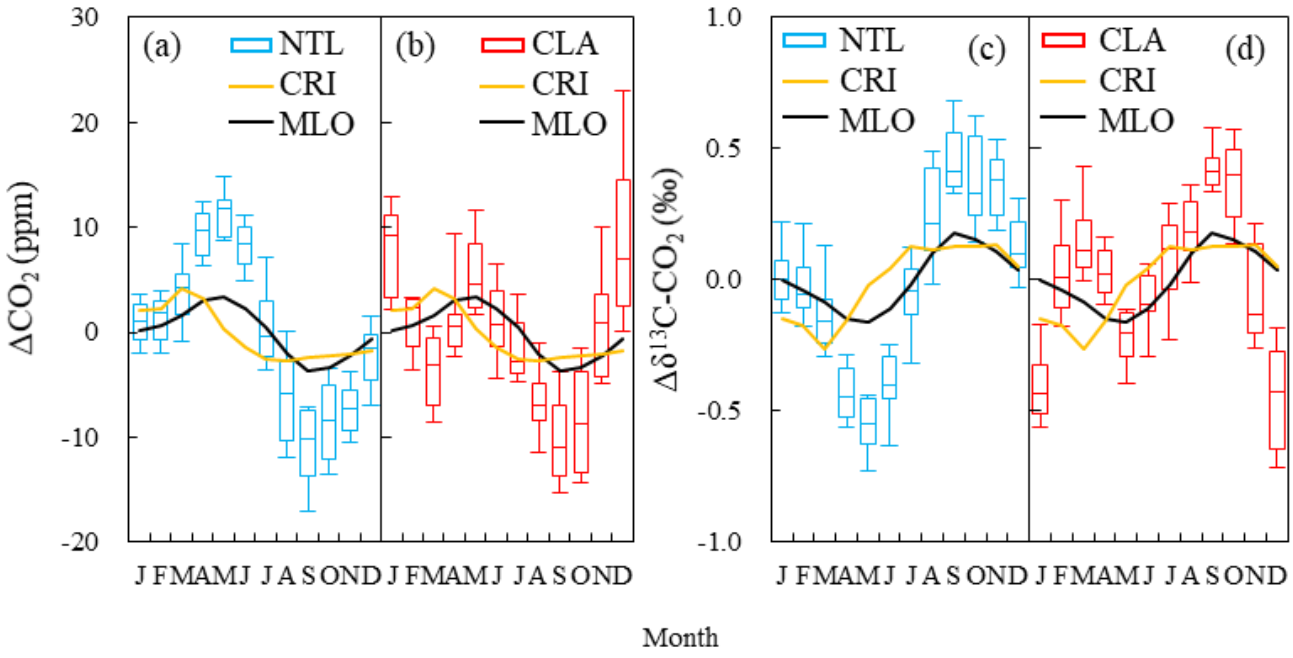

Figure 6. Seasonal variations in the CO_2 mole fraction at (a) Nainital (NTL) and (b) Comilla (CLA) and the isotope ratio of $\delta^{13}C$-CO_2 at (c) NTL and (d) CLA. Boxes with blue and red are for Nainital and Comilla and the black and yellow lines are for Mauna Loa (MLO) and Cape Rama (CRI), respectively. Median values (the line in the box), inner 50th percentile of the value (box), and inner 90th percentile of the value is from the monthly averaged CO_2 mole fractions.

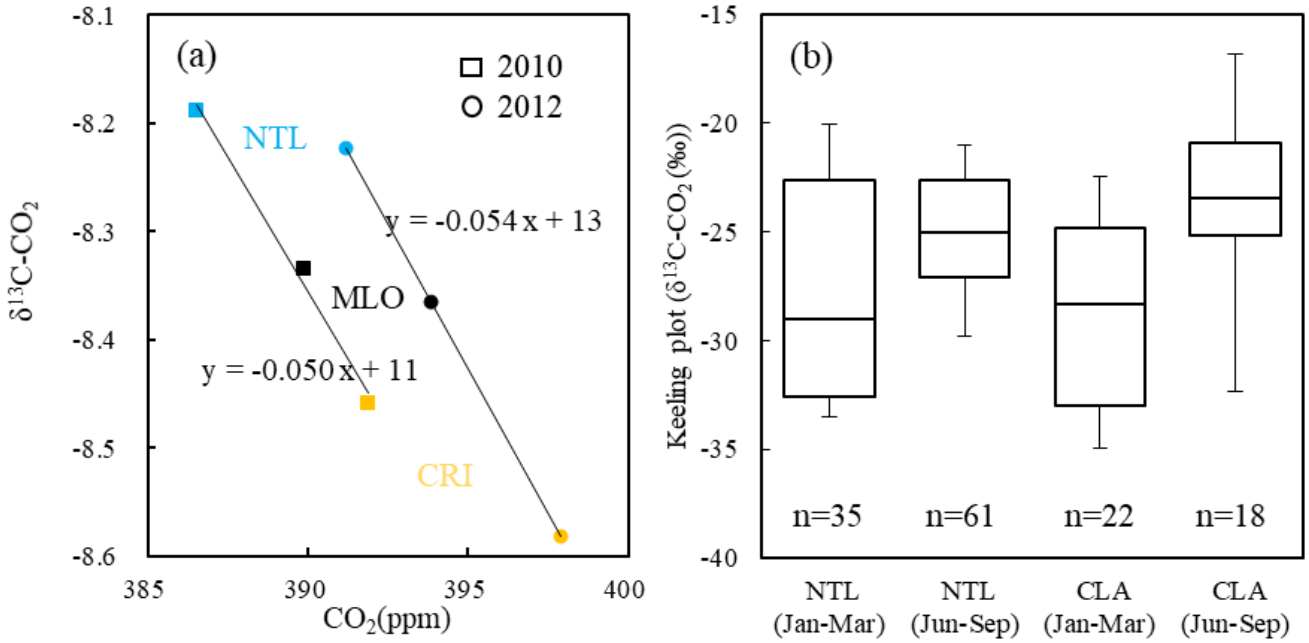

Figure 7. (a) Relationship between the annual values of the CO_2 mole fraction and isotopic ratio of $\delta^{13}C$-CO_2 at Nainital (NTL), Cape Rama (CRI), and Mauna Loa (MLO) in 2010 and 2012, and (b) the intercept values of the Keeling plot of Nainital and Comilla (CLA) in January–March and June–September.

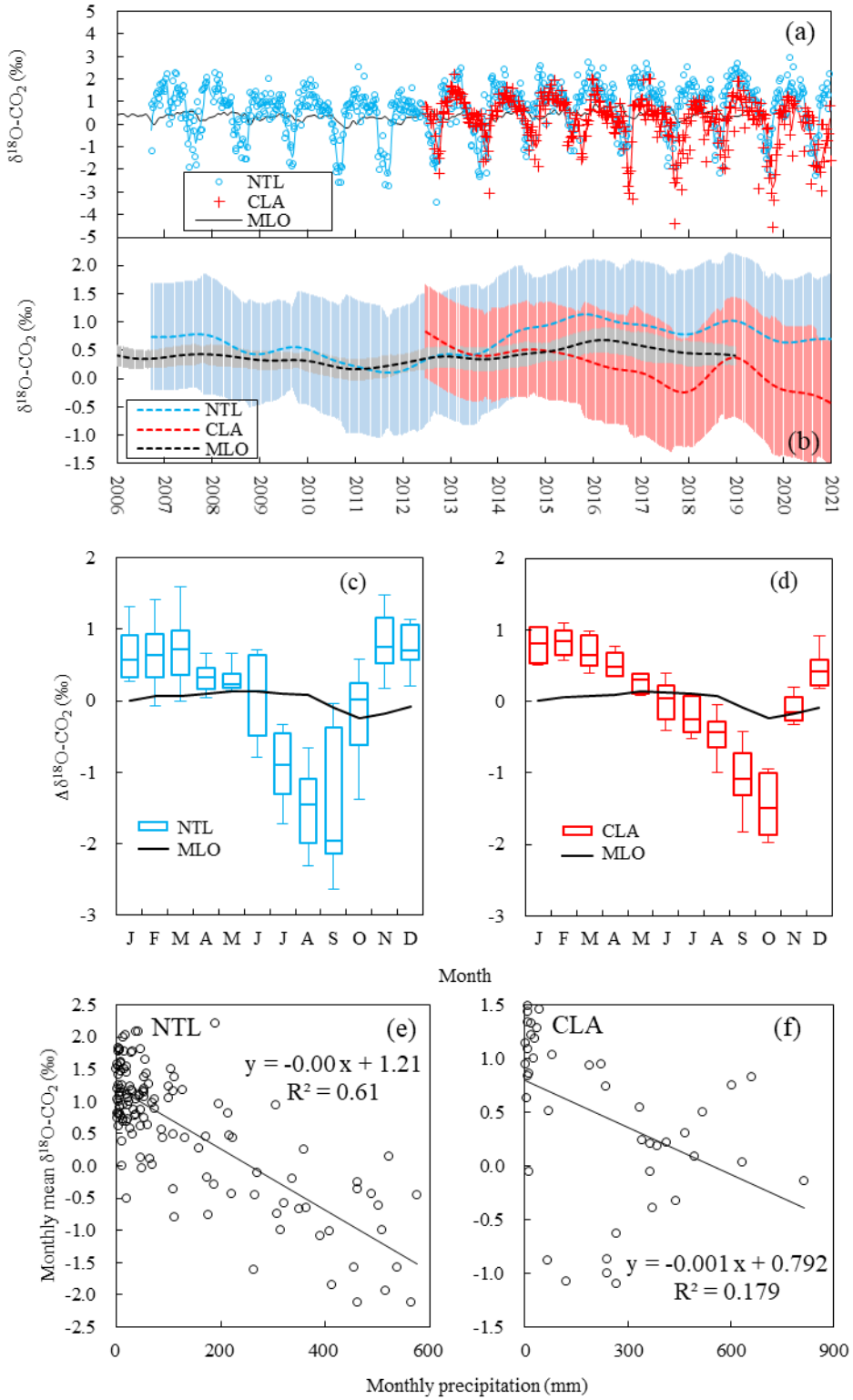

Figure 8. Time series of (a) measured values and (b) long-term trend for isotopic ratio of $\delta^{18}O\text{-}CO_2$ at Nainital (NTL), Comilla (CLA), and Mauna Loa (MLO) in 2006–2020, the seasonal variation of $\delta^{18}O\text{-}CO_2$ at (c) NTL and (d) CLA, and the relationship between monthly precipitation of the state of Uttarakhand and Bangladesh and the monthly mean of $\delta^{18}O\text{-}CO_2$ at (e) NTL and (f) CLA.

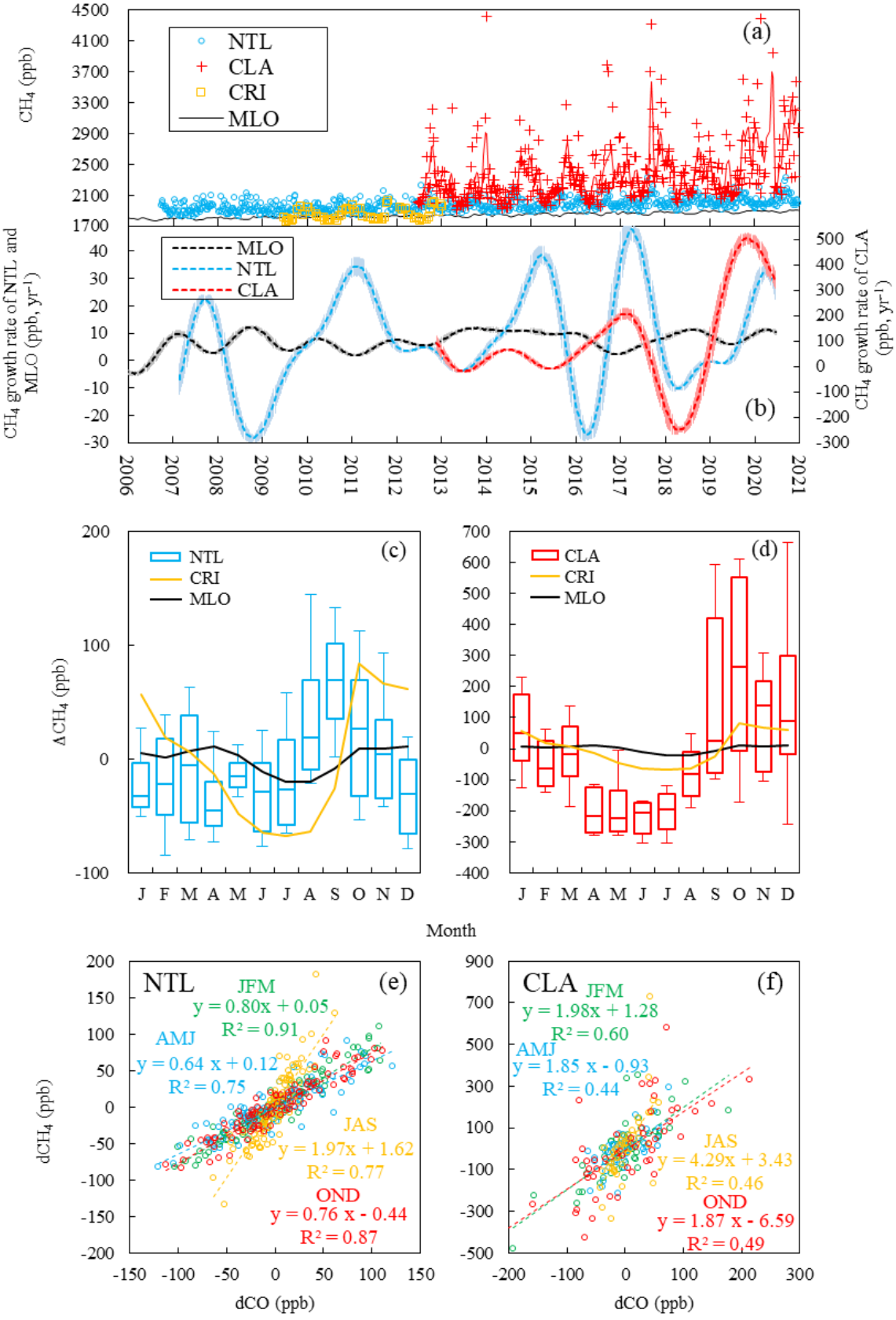

Figure 9. Time series of (a) measured values and (b) growth rate of the CH_4 mole fraction at Nainital (NTL), Comilla (CLA), Cape Rama (CRI), and Mauna Loa (MLO) in 2006–2020, the seasonal variation in the CH_4 mole fraction at (c) NTL and (d) CLA, and the relationship between the short-term component of dCO and dCH_4 at (e) NTL and (f) CLA during January – March (JFM), April–June (AMJ), July–September (JAS) and October–December (OND).

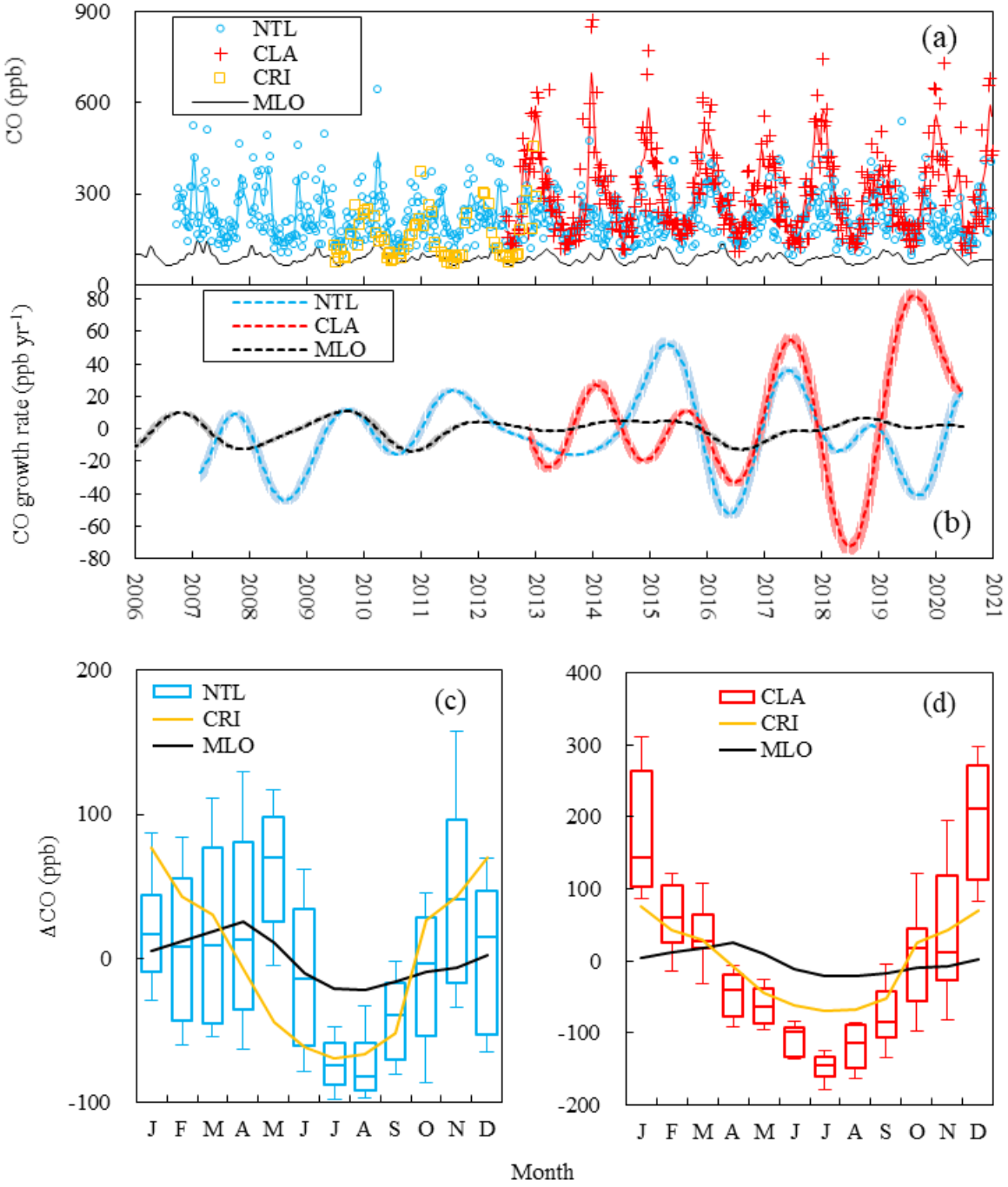

952

953 Figure 10. Time series of (a) measured values and (b) growth rates of CO mole fraction at Nainital (NTL), Comilla (CLA),
954 Cape Rama (CRI), and Mauna Loa (MLO) in 2006–2020, and the seasonal variation of CO mole fraction at (c) NTL and (d)
955 CLA.

956

957

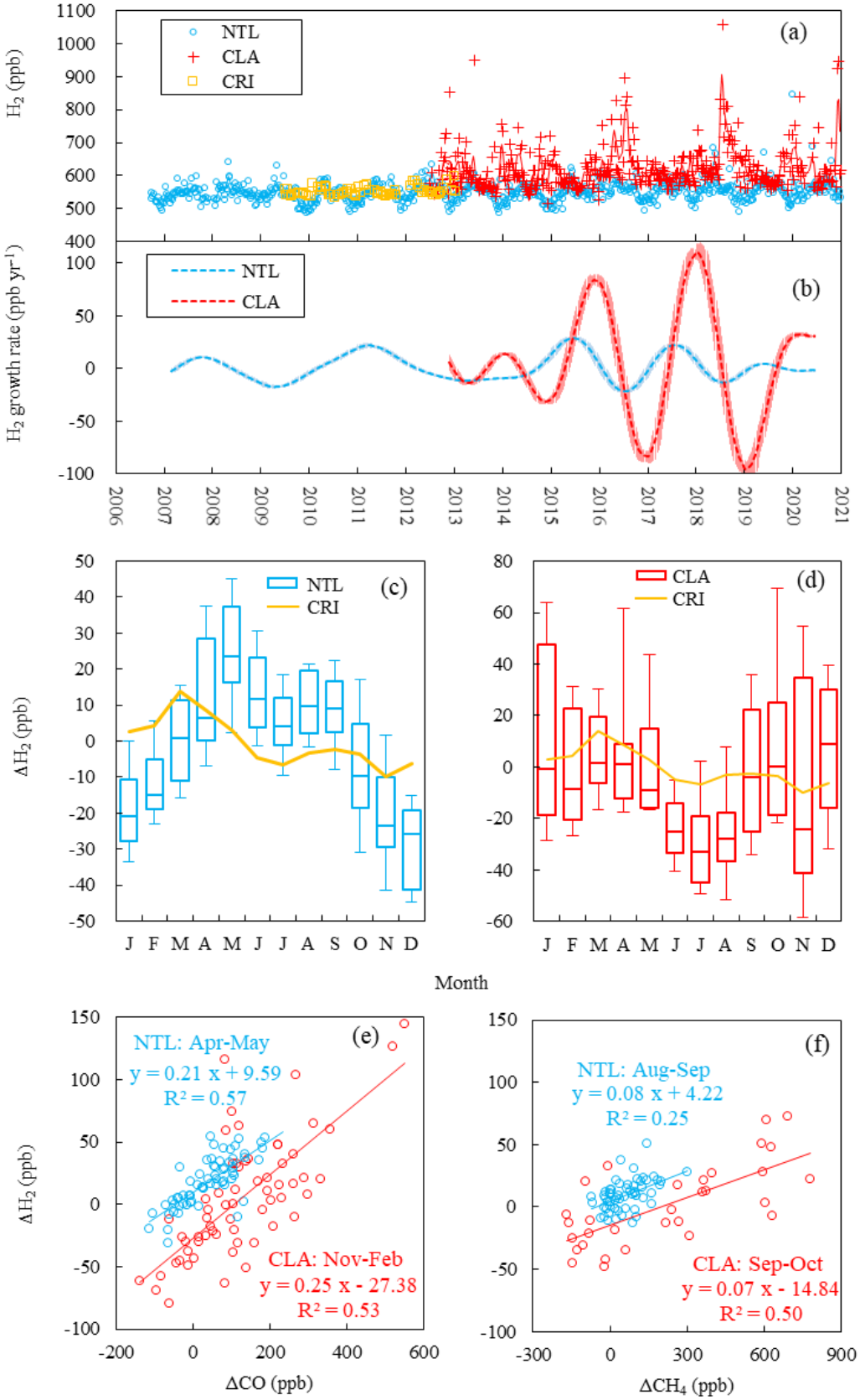

Figure 11. Time series of (a) measured values and (b) growth rate of the atmospheric H_2 mole fraction at Nainital (NTL), Comilla (CLA), and Cape Rama (CRI) in 2006–2020, seasonal variation in the H_2 mole fraction at (c) NTL and (d) CLA, and scatter plots for the relationship of (e) ΔH_2 and ΔCO at NTL during April–May and at CLA during November–February when biomass burning occurred frequently, and (f) ΔH_2 and ΔCH_4 at NTL during August–September and at CLA during September–October when the maximum CH_4 mole fraction was measured.

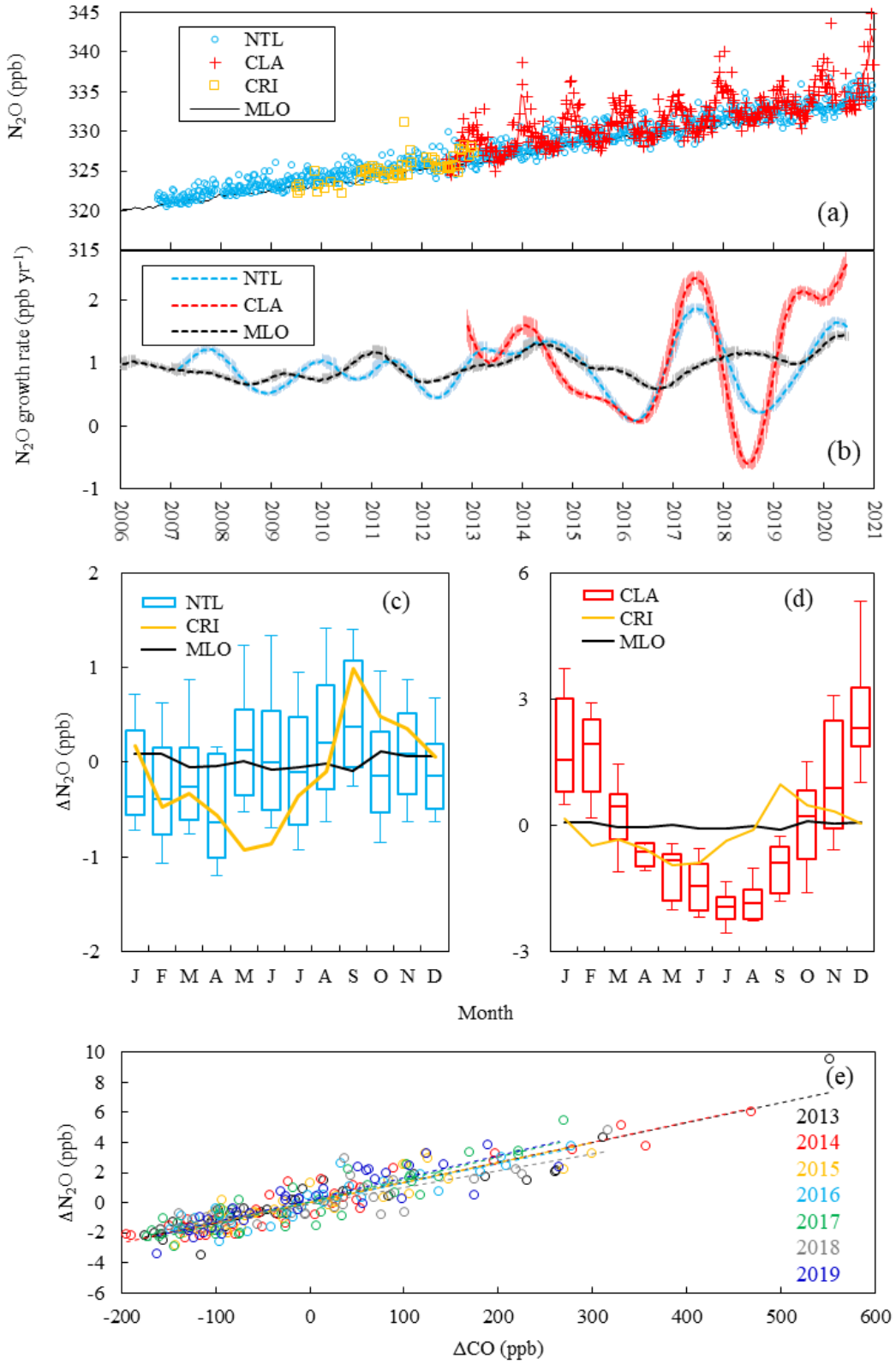

Figure 12. Time series of (a) measured values and (b) growth rates of the N_2O mole fraction at Nainital (NTL), Comilla (CLA), and Mauna Loa (MLO) in 2006–2020, seasonal variations in the N_2O mole fraction at (c) NTL and (d) CLA, and (e) the relationship between the ΔN_2O and ΔCO at CLA in 2013–2019.

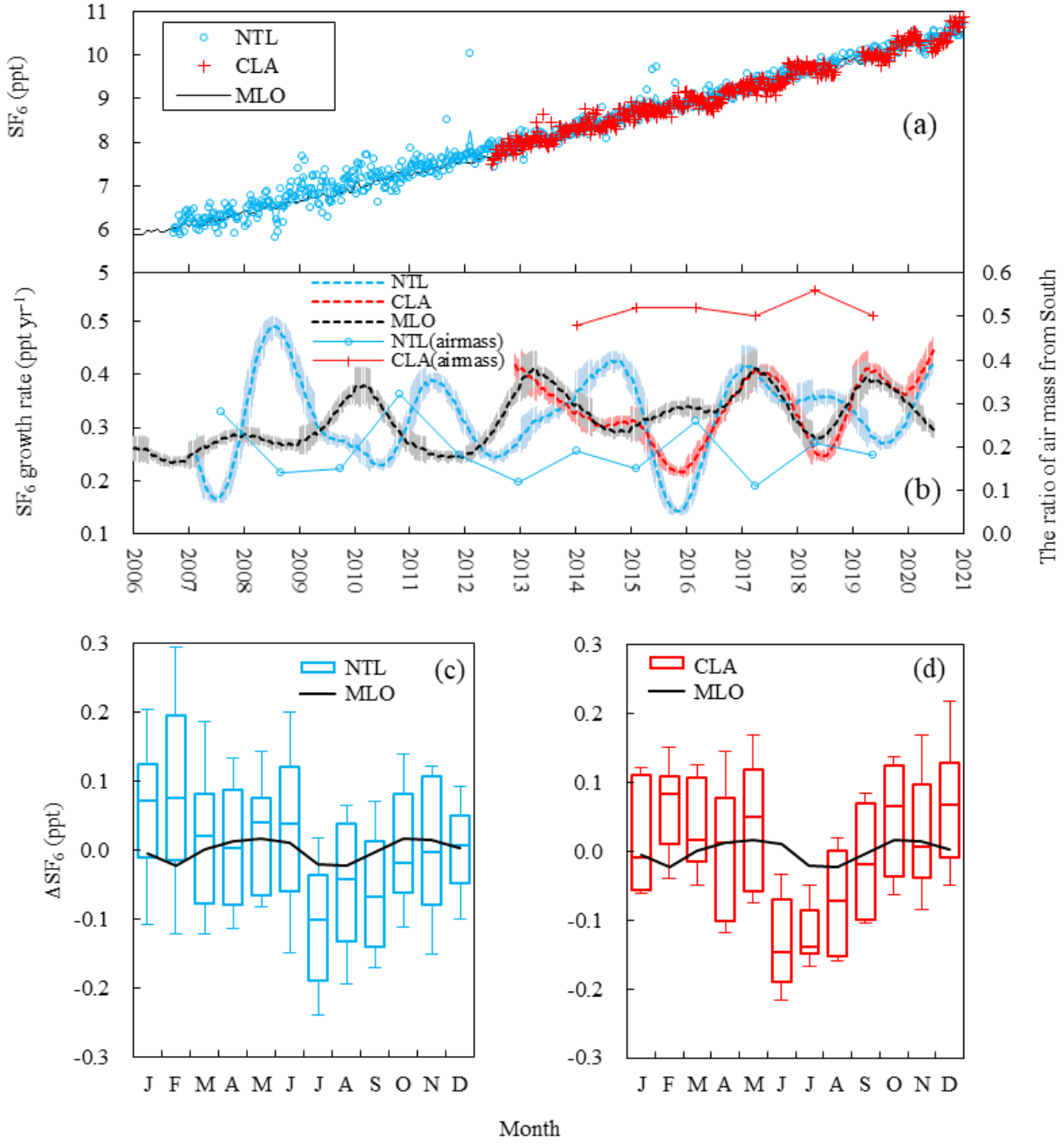

970
971
972 Figure 13. Time series of (a) measured values and (b) growth rates of the SF_6 mole fraction at Nainital (NTL), Comilla
973 (CLA), and Mauna Loa (MLO) and the ratios of the air mass from south at NTL and CLA in 2006–2020, and seasonal
974 variations in the SF_6 mole fraction at (c) NTL and (d) CLA.
975